

From Powder to Pouch Cell: Setting up a Sodium-Ion Battery Reference System Based on $\text{Na}_3\text{V}_2(\text{PO}_4)_3/\text{C}$ and Hard Carbon

Pirmin Stüble,^{*[a]} Cedric Müller,^[a] Nicole Bohn,^[a] Marcus Müller,^[a] Andreas Hofmann,^[a] Tolga Akçay,^[a] Julian Klemens,^[b] Arnd Koeppe,^[a, c] Satish Kolli,^[d] Deepalaxmi Rajagopal,^[a, c] Holger Geßwein,^[a] Wilhelm Schabel,^[b] Philip Scharfer,^[b] Michael Selzer,^[a, c] Joachim R. Binder,^[a] and Anna Smith^{*[a]}

At the research level, novel active materials for batteries are synthesised on a small scale, fabricated into electrodes and electrochemically characterised using each group's established process due to the lack of standards. Recently, eminent researchers have criticised the implementation of e.g. low active material contents/electrode loadings, the use of research-type battery cell constructions, or the lack of statistically relevant data, resulting in overstated data and thus giving misleading predictions of the key performance indicators of new battery technologies. Here, we report on the establishment of a reference system for the development of sodium-ion batteries. Electrodes are fabricated under relevant conditions

using 9.5 mg/cm² self-synthesised $\text{Na}_3\text{V}_2(\text{PO}_4)_3/\text{C}$ cathode active material and 3.6 mg/cm² commercially available hard carbon anode active material. It is found that different types of battery cells are more or less suitable for half- and/or full-cell testing, resulting in ir/reproducible or underestimated active material capacities. Furthermore, the influence of electrode overhang, which is relevant for upscaling, is evaluated. The demonstrator cell (TRL 4–5) has been further characterised providing measured data on the power/energy density and thermal behaviour during rate testing up to 15 C and projections are made for its practical limits.

Introduction

Sodium-ion batteries (SIBs) are considered a promising technology to complement or even replace state-of-the-art lithium-ion batteries. While the anode material of the first commercially available SIBs is expected to be hard carbon,^[1] there are a number of different options for cathode active materials, e.g. Prussian Blue analogues, layered oxides, and polyanionic

materials.^[2] Due to a similar operating principle, SIB's advantage lies in a "drop-in" approach for battery cell manufacturing steps at the electrode level, such as slurry mixing, coating, drying, calendering, as well as at the cell assembly level, taking into account electrode winding/stacking, electrolyte filling and cell formation.^[3] However, the viscosity of the slurry changes due to the change in the active material, which affects the coating process and can lead to different designs of the coating equipment and process parameters (e.g. production speed, film thickness). Furthermore, the influence of binder migration during drying varies in its intensity.^[4] With the same electrode composition, it was found that a slurry containing hard carbon and a water-based binder system (CMC/SBR) leads to less binder migration during rapid drying compared to a standard LIB graphite anode.^[5] Another example is the use of nanoporous structured particles and the binder PVDF, which results in lower adhesion strength of the electrodes compared to electrodes containing compact particles. The advantage, however, is that the electrochemical performance is not impaired during fast drying.^[6] Due to the open porosity of the particles, the binder is distributed over the electrode cross-section and does not clog the pores between the particles. The gravimetric energy density of SIBs has been announced to reach target values of 160 Wh/kg at cell level, which is in the range of LIBs using graphite (Gr) as anode material and lithium iron phosphate (LFP) as the cathode material. Therefore, SIBs are often compared to LFP/Gr batteries and could replace some of the applications of LFP/Gr batteries.^[7] However, there are some differences when comparing LFP/Gr chemistry to SIBs, but the details depend on the

[a] P. Stüble, C. Müller, N. Bohn, M. Müller, A. Hofmann, T. Akçay, A. Koeppe, D. Rajagopal, H. Geßwein, M. Selzer, J. R. Binder, A. Smith
Karlsruhe Institute of Technology (KIT), Institute for Applied Materials (IAM), Hermann-von-Helmholtz-Platz 1, 76344 Eggenstein-Leopoldshafen, Germany
E-mail: anna.smith@kit.edu
pirmin.stueble@kit.edu

[b] J. Klemens, W. Schabel, P. Scharfer
Karlsruhe Institute of Technology (KIT), Thin Film Technology (TFT), Straße am Forum 7, 76131 Karlsruhe, Germany

[c] A. Koeppe, D. Rajagopal, M. Selzer
Karlsruhe Institute of Technology (KIT), Institute of Nanotechnology (INT), Hermann-von-Helmholtz-Platz 1, 76344 Eggenstein-Leopoldshafen, Germany

[d] S. Kolli
Helmholtz Institute Ulm (HIU), Helmholtzstraße 11, 89081 Ulm, Germany

Supporting information for this article is available on the WWW under <https://doi.org/10.1002/batt.202400406>

© 2024 The Authors. *Batteries & Supercaps* published by Wiley-VCH GmbH. This is an open access article under the terms of the Creative Commons Attribution Non-Commercial NoDerivs License, which permits use and distribution in any medium, provided the original work is properly cited, the use is non-commercial and no modifications or adaptations are made.

actual cathode active material being used. In general, SIBs promise faster charging.^[8] Further, they are free of critical metals, such as lithium and cobalt. Of course, they are also free of copper, as aluminium can be used as the current collector material for the cathode and anode, which significantly improves their recyclability.^[9] Because of the latter fact, they can even be deeply discharged and short-circuited for much safer transport conditions, but this is limited to serval electrolyte and cathode compositions of the cell.^[10] Lastly, they offer greater supply independence because they are free of graphite, which is mostly mined in China.^[11]

The above-mentioned arguments for SIBs sound exciting (sometimes in theory). However, for the proof of concept of any functional new battery technology both, cathode and anode active materials combined in a multi-layer electrode full-cell setup must demonstrate sufficient performance under realistic conditions. More specifically, a high active material content and high electrode loadings, as well as proper balancing conditions together with a limited amount of charge carriers originating from the cathode and electrolyte reservoir need to be set to allow for evaluation of energy/power densities and cycle life, temperature behaviour, etc. at the battery cell level. In fact, recent papers have highlighted the importance of putting performance data of newly developed active battery materials from basic research into perspective. Frith et al. criticised the over-extrapolation of early research results as they are "free of several limitations that govern practical applications".^[12] Amine and co-workers summarised a number of crucial test parameters that in their opinion are "often overlooked in academic literature but [that] are critical for practical applicability outside the laboratory" in their publication "Bridging the academic and industrial metrics for next generation practical batteries".^[13] Johansson et al. humorously listed the 'Ten Ways to Fool the Masses When Presenting Battery Research', also highlighting the importance of proper material characterisation, and technologically relevant active material loadings.^[14] Unfortunately, in addition to missing key performance indicators (KPIs) for evaluating new active materials for batteries, there is also a lack of standardisation of test conditions, which has led to discussions within the research community.^[15]

To address these issues, we decided to establish a reference system of well-defined active materials, electrodes and electrolytes for our common SIB research topics, but also to showcase a best practice SIB reference system. In order to increase the benefit to the research community, reference materials have been distributed to 17 research groups and some OEM's across Europe. This work is therefore not an isolated study, but rather a starting point, including a basic characterisation of the benchmark materials, which can serve as a reference for future studies on these materials. For the anode material, we defined and used hard carbon from Kuraray as a benchmark material. On the cathode side, the lack of satisfactory commercial sources for active material motivated us to synthesise our own cathode material, namely carbon-coated sodium vanadium phosphate ($\text{Na}_3\text{V}_2(\text{PO}_4)_3/\text{C}$). The stable cycling behaviour of this SIB chemistry was a key reason why we decided to set the aforementioned active materials as a standard and benchmark

system. In a previous study, after cell formation, discharge capacities of up to 92.6 mAh/g were achieved, and capacity retention >90% over 1000 charge/discharge cycles at 0.5 C/0.5 C could be reached.^[16] The reference electrodes were prepared according to the following KPIs, which are critical for application-relevant performance testing: both the cathode and the anode active material loadings were close to commercial standards, >90 wt % active material loadings were realised with 3.6 mg/cm² hard carbon (~1.2 mAh/cm²) and 9.5 mg/cm² NVP/C (~1.0 mAh/cm²). For full-cells, the balancing of the negative/positive capacity ratio (N/P ratio) has been adjusted for initial loss of sodium-ions during formation and was kept as close to 1 as possible to maximise the total energy density. However, the total capacity of the hard carbon electrode slightly exceeds that of the NVP/C electrode to avoid any sodium plating.

In the second part of this study, we present the results of a round robin study on the reference electrodes, where four different types of laboratory cell formats are compared. Using different types of half-cells, either the cathode or anode is installed against elemental sodium to obtain individual readings for potential curves, specific ir/reversible capacities, and initial/following coulombic efficiencies (ICE/CE) of the respective electrodes. Coin cells or similar commercially available two- or three-electrode cell configurations were used for this purpose. This was motivated by the fact that reliable electrode capacity measurements are the key to correctly adjust the balancing of the full-cell. As recently demonstrated, it is surprisingly challenging to obtain reproducible and correct data from half-cells measurements against elemental sodium, especially with hard carbon electrodes.^[17]

As degradation/aging may be caused by different factors in SIB systems compared to our recent LIB study,^[18] we were keen not only to compare the electrochemical data obtained in (different types of) sodium-ion half-cells, but also to examine and contrast the results obtained from coin cells, single-layer and multi-layer pouch cells to one another in full-cell configuration. Finally, pilot-level battery cells, namely single-layer (~19 mAh after formation) and larger footprint area multi-layer pouch cells (~3.5 Ah after formation) are used to validate full-cell characteristics, such as ICE/CE and initial cycling stability.

Results and Discussion

NVP/C Active Material Specifications

From the synthesis described in the experimental section, a total of 2.5 kg of the NVP/C cathode active material was synthesised. SEM images of the active material are shown in Figure 1. As reported previously^[19] NVP/C is a composite material consisting of carbon-coated nano-crystalline NVP primary particles. As a result of the spray-drying synthesis and calcination, the particles are agglomerated in the form of porous spherical granules, as shown in Figure 1. The corresponding pore size distribution is shown in Figure 2a. In accordance with the cross-sectional SEM images of the material, pore diameters of <300 nm were attributed to pores inside

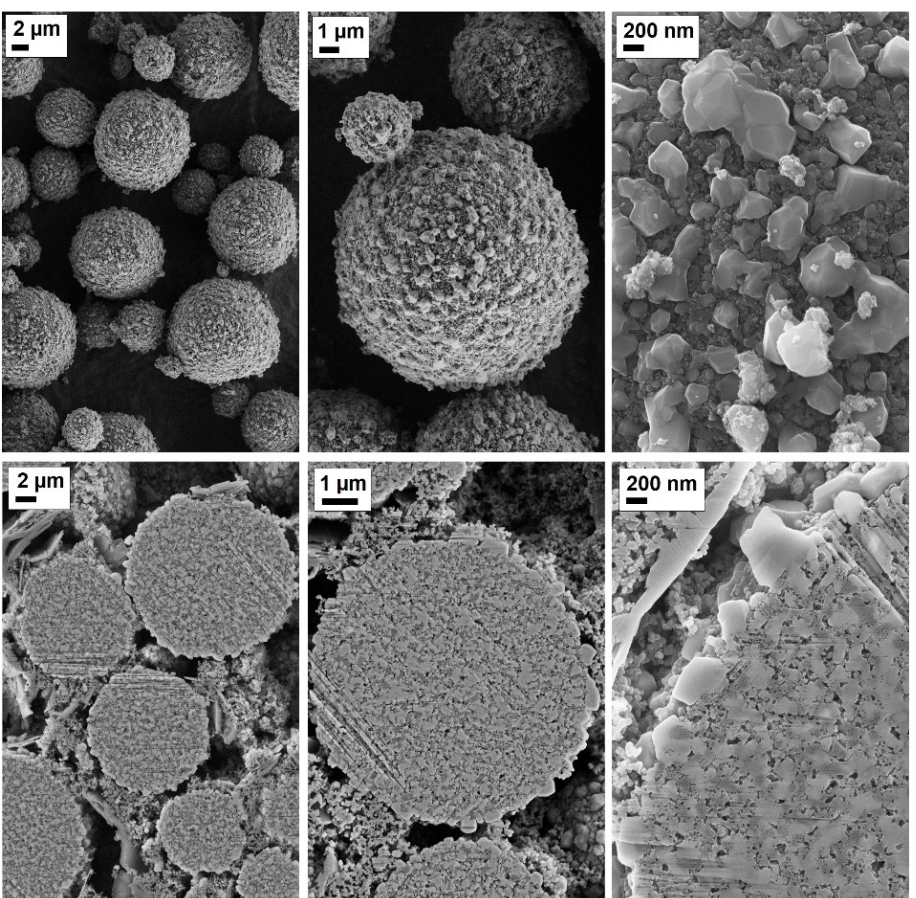


Figure 1. SEM images of the NVP/C active material (top). SEM images of cross-sections of NVP/C (bottom), revealing the porous structure of granules which consist of NVP primary particles embedded in a carbon matrix.

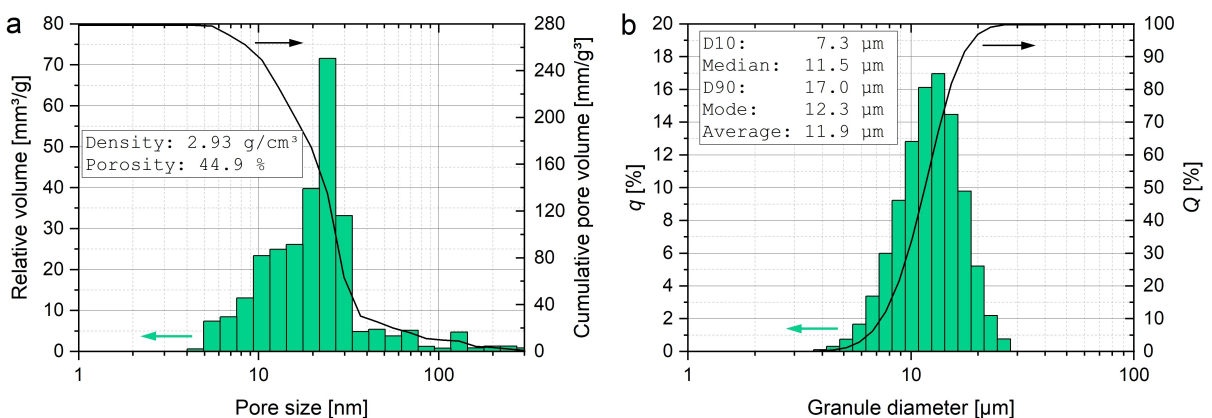


Figure 2. a) Size distribution of nano-pores inside the NVP/C granules (determined by mercury intrusion porosimetry). b) Volumetric particle size distribution for the NVP/C granules (determined by laser scattering).

granules. The corresponding cumulative pore volume of 278 mm³/g, yields an internal porosity of 44.9%, based on the density of the NVP/C active material of 2.93 g/cm³, which was determined by means of He-gas pycnometry. The specific surface area of the material was determined to be 96.5 m²/g.

The secondary particle size distribution of the active material was determined by laser scattering and is shown in Figure 2b. The spherical granules obtained from the final

calcination process have diameters ranging from 7.3 μm (D_{10}) to 17.0 μm (D_{90}) with an average value of 11.9 μm. The carbon content of the active material was determined to be 11.2 wt % by means of elemental analysis. For NVP, the stoichiometry $\text{Na}_{3.00}\text{V}_{1.99}(\text{PO}_4)_{3.01}$ is found, which confirms the ideal composition within the scope of the measurement accuracy. A table with detailed analysis results can be found in the Table S1 in the supporting information (SI).

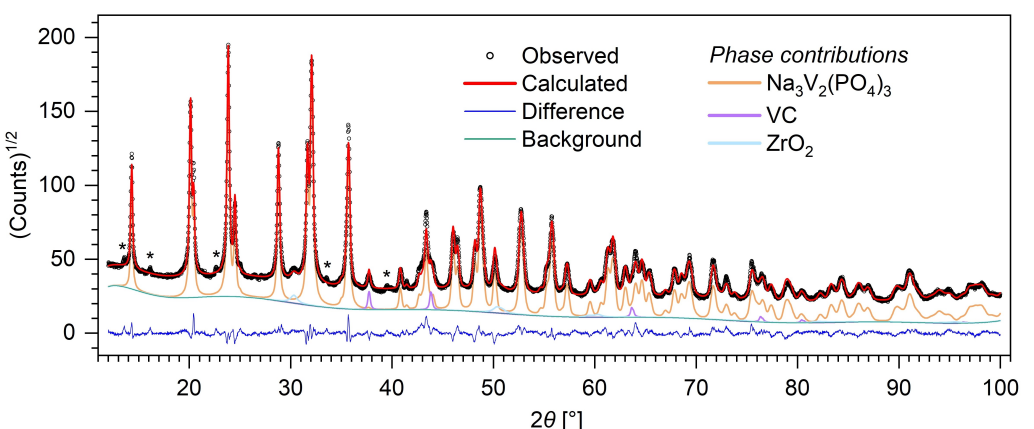
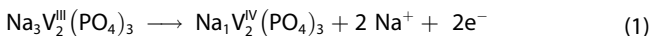


Figure 3. Powder X-Ray diffraction pattern and Rietveld refinement of the NVP/C cathode active material. For the sake of clarity, the background and individual phase contributions have been set off vertically by 15 counts. Reflections marked with an asterisk could not be assigned.

The X-ray diffraction pattern together with the Rietveld refinement results of the synthesised NVP/C composite cathode material are shown in Figure 3. The average crystal structure of the NVP phase can be described by the rhombohedral $\bar{R}\bar{3}c$ NaSICON-type structure,^[20] with refined lattice parameters of $a=b=872.73(2)$ pm and $c=2186.14(8)$ pm. The estimated primary crystallite size calculated from a double-Voigt approach as implemented in the TOPAS software is 121(3) nm.^[21] In addition to the main NVP phase, small amounts of tetragonal zirconium dioxide (ZrO_2) and vanadium carbide (VC) are also present in the synthesised composite. Based on the Rietveld refinements the weight fraction of ZrO_2 is 1.0% and that of VC is 0.7%. The ZrO_2 originates from the grinding debris of the used ZrO_2 milling balls used and the VC originates from the synthesis process as we have described in a previous publication.^[22] Despite comparison with common databases like ICDD-PDF, COD and ICSD, we were not able to find any phases that match the weak reflections at 13.6° , 16.1° and 22.6° . However, based on the weak diffracted intensities, we estimate the phase fraction of the unidentified impurity below 1 wt%, so the influence on the calculated capacity should be minimal.

The theoretical capacity of pure NVP corresponding to the V^{IV}/V^{III} redox couple occurring at a potential of ~ 3.4 (vs. Na/Na^+) according to Equation (1) is 117.6 mAh/g (NVP).



However, this capacity cannot be achieved on material level, since the composite material contains 11.2 wt% carbon and secondary phases (~ 2 wt%). Taking these electrochemically inactive components into account, a capacity of 102.1 mAh/g is expected for the NVP/C active material investigated herein. Despite the fact that NVP/C is not a perfectly phase-pure material, the advantages of using it as a reference material for research are obvious: NVP/C has good electrochemical properties and shows excellent cycling stability,^[16] but more importantly, it is possible to produce this material with reproducible properties on a kg scale.

Hard Carbon Active Material Specifications

As anode active material, commercial hard carbon (HC), namely Kuranode Type II, 9 μm (Kuraray) was used. According to the material data sheet,^[23] the first charge capacity of the material is 332 mAh/g (0.1 mA/cm² constant current (CC), with a constant voltage (CV) phase at 0 V until $I < 0.02$ mA/cm²). Note that the electrode loading is not specified and thus it is not possible to calculate the C-rate, which was used to determine this capacity. The 1st discharge capacity is stated to be 298 mAh/g. The irreversible capacity loss is reported to be 34 mAh/g corresponding to an ICE of 89.8%. The charge capacity could be confirmed experimentally previously^[17] and in the present study. The discharge capacity and thus the ICE value could not be fully reproduced, which however will be discussed in detail below.

Electrolyte Specifications

As listed in Table 1, electrolytes based on a mixture of ethylene carbonate (EC) and propylene carbonate (PC) with the conductive salt sodium hexafluorophosphate ($NaPF_6$), and, in the case of the half-cells, the additive fluoroethylene carbonate (FEC) were used for the investigation of the HC and NVP/C electrodes. The electrolytes were selected based on the results of a previous electrolyte screening^[17] and, in the case of the full-cell electrolyte without FEC, based on the proven long-term cycling stability.^[16] Our selection is confirmed by more recent studies, which likewise conclude that FEC is not a suitable additive for NVP vs. HC full-cells.^[24] The water content of the

Table 1. Electrolyte composition used in half- or full-cells.

Electrolyte	Composition
Type A (half-cell electrolyte)	1 M $NaPF_6$ in EC/PC (1:1, wt%) + 5 wt% FEC
Type B (full-cell electrolyte)	1 M $NaPF_6$ in EC/PC (1:1, wt%)

electrolyte B was determined to be below 20 ppm by means of Karl-Fischer titration. Details of the electrolyte preparation are provided in the experimental section.

Electrode Properties

The often drastic differences between electrode formulations and loadings in research papers compared to technologically relevant electrodes were already addressed in the introduction. Results obtained from ultrathin research electrodes cannot easily be extrapolated to the properties of electrodes with technologically relevant active material loadings. To tackle this issue, and to create a reliable basis for realistic projections, areal capacities of 1.0 and 1.2 mAh/cm² for the cathode and anode, respectively, were defined as target values for the reference electrodes. As shown in Table 2, and as discussed in the later

section of the round robin studies, these values were achieved in good approximation.

The NVP/C cathode was prepared from a slurry based on *N*-methyl-2-pyrrolidone (NMP), which was coated on an aluminium foil using the doctor blade technique. From 250 g of active material, 16 m of homogeneous cathode was obtained. The hard carbon anode was prepared in an aqueous process and coated on aluminium foil using a slot die. From 100 g of active material used, around 20 m of homogeneous electrode with a width of 14.5 cm were obtained. Details of the slurry preparation and coating process can be found in the experimental section. The thicknesses of the electrodes before and after calendering, together with other electrode properties, are listed in Table 2.

A cross-section of the calendered hard carbon anode is shown in Figure 4a. In addition to the compact angular hard carbon active material particles, carbon black is visible in the form of fine flakes. The thickness of the coating layer from the

Table 2. Summary of the electrode properties. ^{*1}Electrode loadings (and corresponding estimated standard deviations, in brackets) were determined based on each 32 electrodes investigated in a round robin study (see below). ^{*2}Thicknesses were determined using micrometre calliper. ^{*3}Areal capacities are calculated based on theoretical capacities of 332 mAh/g for hard carbon and 102.3 mAh/g for the NVP/C composite material. Experimental capacities are discussed below.

Electrode properties		Cathode	Anode
Active material	type	NVP/C	HC
	content	[%]	90.5
Electrode loading ^{*1}	total	[mg/cm ²]	10.4(3)
	active material	[mg/cm ²]	9.5(3)
Dry film thickness ^{*2}	before calendering	[μm]	118(9)
	after calendering	[μm]	99(1)
Porosity	before calendering	[%]	67.8 (1.1)
	after calendering	[%]	61.6 (1.3)
Current collector	material		Aluminium
	thickness	[μm]	15
	mass	[mg/cm ²]	4.1
Areal capacity ^{*3}		[mAh/cm ²]	0.97
			1.18

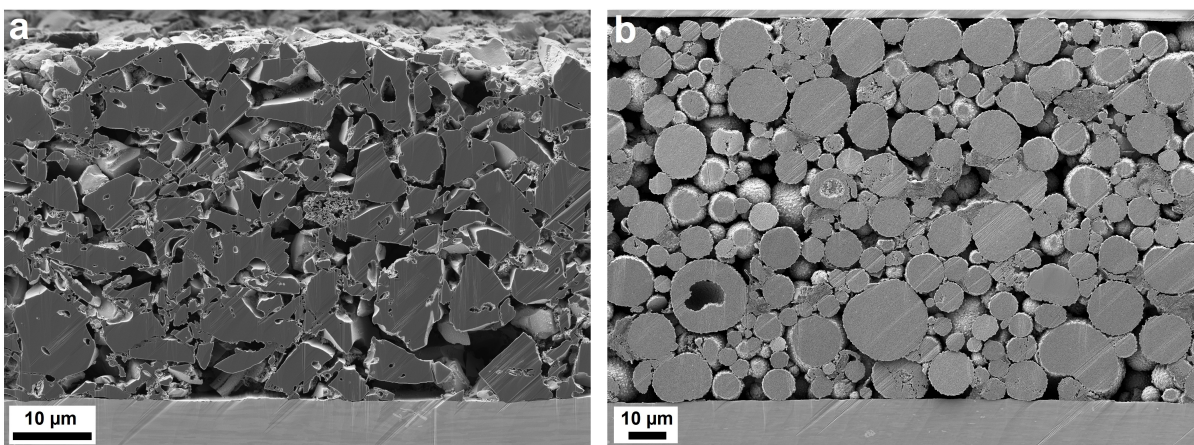


Figure 4. a) Cross-sections of the hard carbon anode. The aluminium current collector is visible at the bottom of the image. b) Cross-section of the NVP/C cathode. As an artefact of the sample preparation, a glass slide is visible at the top of the image. Note the different magnifications of a) and b) (1500 x and 700 x, respectively).

SEM image is $\sim 44 \mu\text{m}$, which is in good agreement with calliper measurements. Due to the rather large primary particle size and inflexibility of the hard carbon particles, the electrode could only be calendered to a very limited extent, so that a rough surface and rather high porosity remains. The NVP/C electrode coating is about twice as thick as the hard carbon electrode coating. A cross-section of the calendered cathode is shown in Figure 4b. Only very few of the originally spherical NVP/C granules are deformed and cracked, as a result of the densification process. The cathode coating layer thickness measured from the SEM image is $100 \mu\text{m}$. The surface of the electrode appears relatively smooth. The porosity of the cathode remains quite high ($\sim 62\%$) even after calendering, which has two reasons. Firstly, the spherical NVP/C particles themselves have a porosity of 45% (see above), and secondly, the cathode was only slightly calendered. The latter improves processing properties, such as reduction of delamination/excessive wrinkling of electrodes. For the NVP/C cathode in particular, we assume that the electrode could still be significantly optimised by reduction of the carbon content within the active material,^[22] increase of the overall active material content in the electrode, and reduction of the electrode porosity. This would lead to higher energy densities (see below), but is beyond the scope of this work.

Reference Material Distribution for Round Robin Studies

Not only for this study, but also for further research activities, active material powders, electrodes (see Table 6, and Figure 5) and electrolytes have been distributed to affiliated groups of the POLiS research Cluster, as well as to some OEMs and external research groups within Europe (total of 17 participants). In order to obtain a realistic impression of the required material and electrode quantities, a demand enquiry was carried out prior to material procurement and electrode production.

Standardisation of SIB materials, that is, coordinated procurement and distribution, offers a number of advantages:

- (1) The materials can be used as a benchmark, for instance when investigating other SIB active materials, electrodes, electrolytes/additives or inactive components.
- (2) With the results presented in this work, a comprehensive characterisation of active materials, electrodes and electrolytes is provided. This eliminates the need to repeat the basic characterization steps within upcoming research activities.
- (3) The central procurement or production and distribution of materials ensures that different groups work with the same batch of the same active material, and equally processed electrodes. Differences originating from material or electrode processing can therefore be excluded.
- (4) The reference materials can be used to check the reproducibility of measurement methods and evaluation procedures.

Of course, there are also some difficulties and disadvantages, which, for the sake of completeness, likewise should be mentioned:

- (1) It requires planning, coordination and time to produce, characterise and distribute materials. In the present case, it took about seven months from demand enquiry to delivery of the materials.
- (2) Research institutes may lack the facilities to prepare materials in large quantities and to manufacture electrodes.
- (3) The quantities of materials and electrodes that are actually required may deviate from planned amounts, which can lead to material shortages.
- (4) The shipment of materials in some cases may be associated with administrative and logistical difficulties.

As mentioned above, the need to provide some standard materials for SIB research is mainly due to the lack of high quality commercially available cathode active materials and electrodes that can be used for scientific work. We therefore believe that in the current situation, the advantages of setting up a reference system outweigh the disadvantages. With the increasing commercialization of the technology, this problem

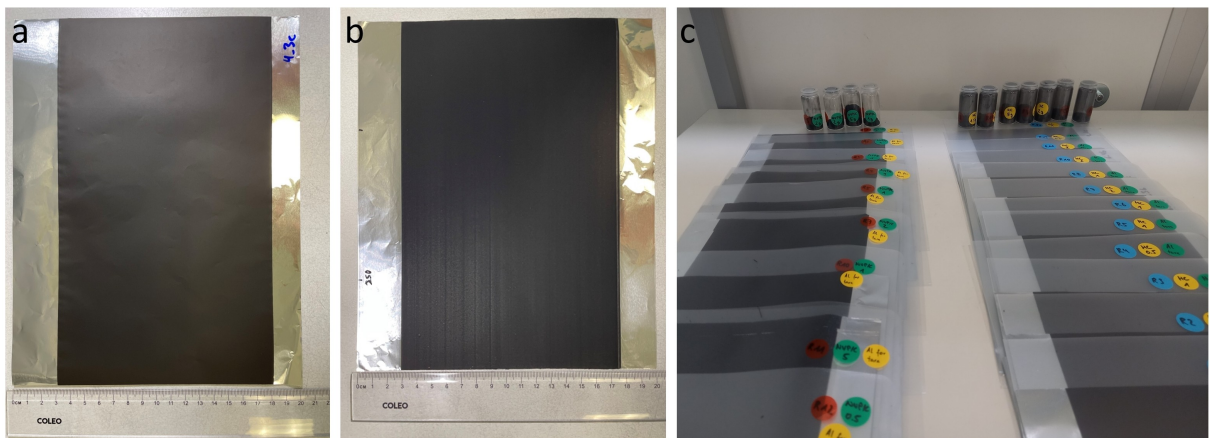


Figure 5. Photos of a) a sheet of the hard carbon reference anode, b) a sheet of the NVP/C reference cathode and c) the preparation for the distribution of active material powders and electrodes for further studies.

may become obsolete in the coming years, when standard materials and electrodes may be established and commercially available without legal restrictions.

Round Robin (RR) Study

Round Robin Study and Data Management

To investigate the electrochemical properties of the NVP/C and the hard carbon electrodes, a round robin study with three research groups and four cell formats was conducted. All groups were given the standard electrodes and electrolyte. The task was to build each four HC half-cells (part A), four NVP/C half-cells (part B) and four NVP/C vs. HC full-cells (part C). Directly after assembly, the cells were delivered to a central test stand equipped with a climate chamber for testing. The four different cell formats, namely 2E Patt cells (a), 2E Swagelok cells (b), 2E 2032 coin cells (note that the notation "CR2032" is not used, because C corresponds to a lithium-ion based cell chemistry, (R stands for round, 20 indicates the diameter of 20 mm and 32 the thickness of 3.2 mm)) (c) and 3E Swagelok cells (d) are shown in Figure 6.

Cell types (a), (b) and (c) were built in two-electrode (2E) configurations, namely working electrode (WE) against counter electrode (CE), resulting that the counter electrode (CE) is also the reference electrode (RE). Thus, the cell voltage (E_{cell}) is used as the control voltage. Cell type (d) was used in three-electrode (3E) configuration with sodium metal as RE and in half-cells also as CE. The potential for the galvanostatic cycling of the half-cells is controlled by the voltage between the WE and RE, while the cell voltage was used to control the cycling of the full-cells. For a detailed comparison of the individual cell configurations, the reader is referred to Nölle et al.^[25]

Cell type (a) is a commercial and reusable cell from EL-CELL (Germany),^[26] that has been developed for use in the three-electrode configuration. However, as no suitable sodium reference electrodes were initially available, only the two-electrode configuration was used. 2032 coin cells (c) are probably the most common cell format in battery research, and

have been discussed extensively in a previous work.^[18] Cell types (b) and (d) are 1/2" reusable commercial two and three-electrode cell types (Swagelok, USA). Further details on the cells and cell assembly are given in the experimental section.

For all battery cells, four constant current cycles at C/10 followed by a CV-phase (until $I < C/20$) during the charging step were applied as formation procedure. The full-cells were additionally cycled for 100 cycles at 0.5 C (charging and discharging current, in charging direction with CV-phase). Voltage windows were 0.005–2 V for the HC and 2.3–3.9 V for the NVP/C half-cells and for the full-cells. Detailed information on the cycling conditions and hardware are given in the experimental sections. We use the terms 'charge' and 'discharge' according to the ion transport in the full-cell. Therefore, in half-cells, 'charging' for NVP/C refers to desodiation of the NVP/C material, while 'charging' for HC refers to sodiation of hard carbon material and vice versa.

For each part of the round robin study, four cells of each type were assembled and cycled. Full datasets, including inaccurate and irreproducible measurements are shown to provide detailed insights into each experiment. All cell tests were unambiguously labelled, e.g. "A_03-01". Herein, the letter A stands for part A (of A, B, C) of the study, the first two-digit number represents the cell type (02: Patt cell; 03: 2E Swagelok cell, 04: 2E 2032 coin cell; 05: 3E Swagelok cell) and the second two-digit number 01 to 04 displays the test number. The active material loadings for the individual cell tests are listed in Table S2.

The research data infrastructure Kadi4Mat^[27] has already proven to be a useful tool for round robin studies.^[28] Therefore, based on the identifier, all data are stored in as linked records in a collection for the study. The associated metadata are collected manually based on a minimalistic domain schema and enriched with automatically extracted metadata. The automatic (meta)data extraction pipeline for BioLogic battery cycle files uses a newly developed Python module that leverages an updated version of the yadg module.^[29] The suggested changes to yadg were collected and shared in a merge request with the developers. Finally, the data extraction pipeline automatically generates figures and reports for overview records in Kadi4Mat.

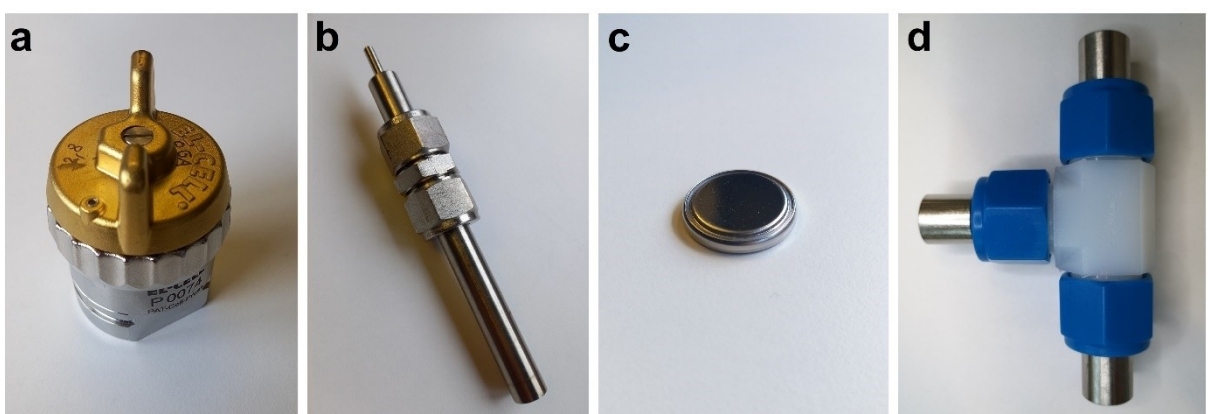


Figure 6. Laboratory research cell types used during the round robin test for the characterisation of the NVP/C and HC electrodes. a) 2E Patt cell, b) 2E Swagelok cell, c) 2E 2032 coin cell and d) 3E Swagelok cell.

Through the Kadi4Mat's Zenodo integration, all data were published as RO-crate data format^[30] under <https://doi.org/10.5281/zenodo.12165686>.

In future work, the existing knowledge graph and metadata description will be adapted and expanded to conform with the Battery Interface Ontology (BattINFO)^[31] and Elementary Multi-perspective Material Ontology (EMMO)^[32] ontologies by integrating the existing structures and domain schema. Furthermore, the reports and overview records will be made interactive through the implementation of dashboards in Kadi4Mat.

HC Half-Cells (RR-part A)

Hard carbon vs. sodium metal half-cells were built using the FEC containing electrolyte type A. All coulombic efficiencies and specific capacities for four formation cycles at C/10 are shown in Figure 7. In addition, the potential curves of all individual cells are shown in Figure S1 (SI). With regard to the application of HC in full-cells, it is essential to correctly determine the capacity, specifically the first charge capacity, of hard carbon electrodes to properly adjust the N/P ratio.^[17] It becomes obvious from Figure 7 that only in one cell format, namely the three-electrode Swagelok cell, a reasonable capacity of

338(5) mAh/g or 1.207(19) mAh/cm², respectively, is measured, that can be reconciled to the manufacturer's specifications of 332 mAh/g^[23] and the calculated areal capacity of 1.18 mAh/cm² (see above).

Highly reproducible test results are also obtained from 2E Swagelok cells, however, with 315(5) mAh/g and 1.125(19) mAh/cm², the capacity is somewhat underestimated. The two other 2E configuration type cells, namely the Patt cells and 2032 coin cells clearly failed by underestimating dis/charge capacities by half to two thirds of the actual electrode capacity. For the sake of completeness, the mean values including the estimated standard deviations (e.s.d.) are noted in Figure 7. Further, the individual measurements of the Patt cell and coin cell format are significantly less reproducible, thus we do not consider these to be meaningful findings.

The manufacturer's specified discharge capacity of 298 mAh/g and the associated high ICE of 90% is not achieved in any of the cell formats. A plausible reason, however, might be the deviation in concentration of NaPF₆ conducting salt and solvent used by the manufacturer, as well as the different discharge current and CV-conditions used in this study (C/10 and CV at 5 mV until I < C/20) compared to the manufacturer's settings (0.1 mA/cm² and CV at 0 V until I < 0.02 mA; due to the lack of active material loading information the C-rate cannot be

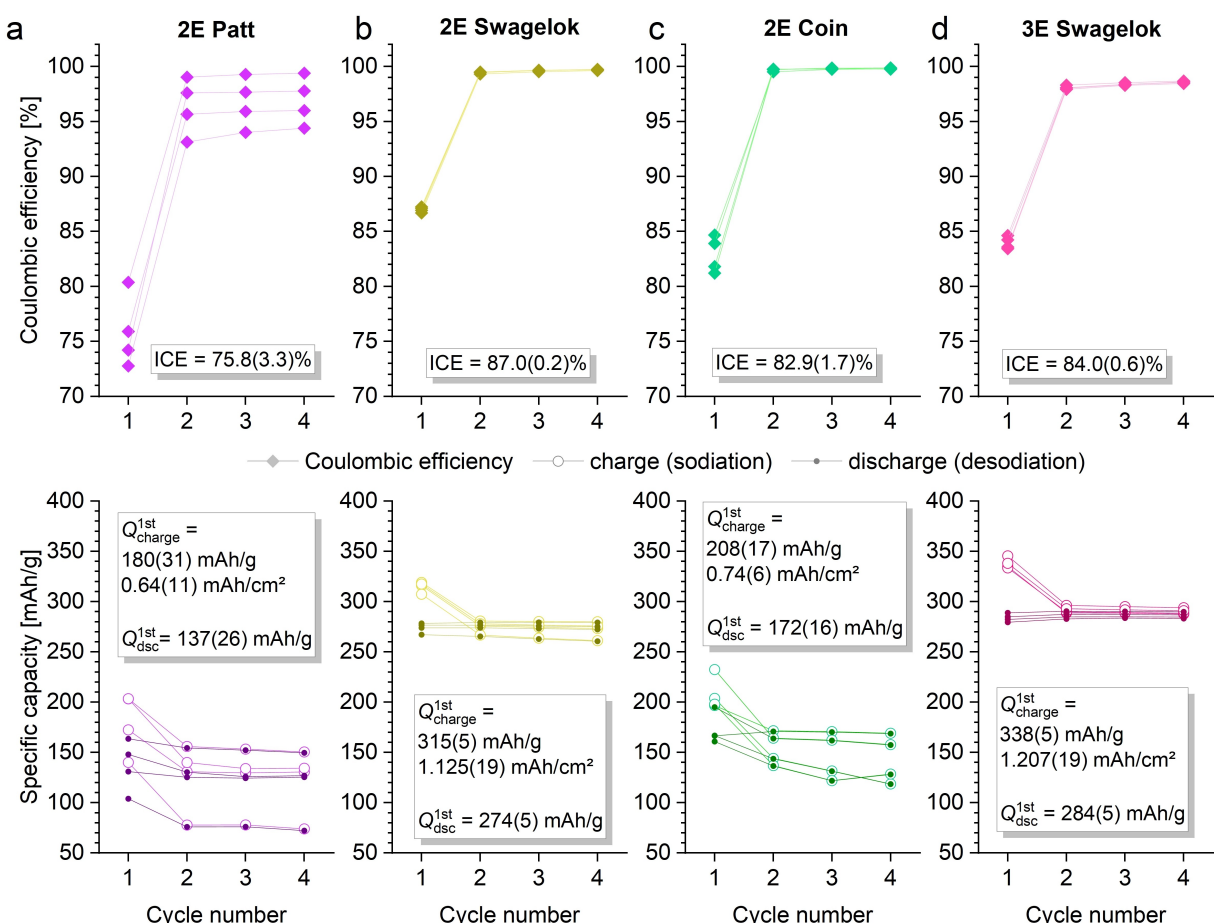


Figure 7. HC vs. sodium half-cell formation results from four C/10 cycles: top panels display coulombic efficiency, while bottom panels visualize the specific capacity of each dis/charge cycle measured.

determined unambiguously).^[23] In the round robin study, the highest ICE of 87% with an e.s.d. of only 0.2% is observed in the 2E Swagelok cell. Reasonably high and reproducible ICE values of 82.9(1.7)% and 84.0(0.6)% are also observed in the coin cells and 3-electrode Swagelok cells, respectively. The significantly reduced value in the Patt cell (ICE=75.8(3.3)% might be due to ongoing side reactions, which may have been facilitated by errors during cell assembly or faulty contacting of the cells. The circumstance that both, Patt cells and coin cells show reasonable CE values, but significantly underestimated capacities, indicates that charging and discharging is highly reversible, but the hard carbon active material simply cannot be fully charged. The reason for the underestimation of the HC capacity is most likely due to over-potentials^[17] at the sodium counter electrode and internal resistance of the cells. Hence, the lower voltage limit of 5 mV is reached prematurely, which results in incomplete charging.

Remarkably, the 2E Swagelok cells, deliver both, very good ICE values and quite reasonable capacities. A possible explanation could be that sodium was directly rolled onto the current collector stamp by the researcher, unlike for other cells, where it was simply placed onto the current collector. The former procedure supposedly creates a tight connection between the alkali metal and the current collector. For the latter procedure, a

gap remains between sodium and current collector, into which electrolyte can penetrate and react at the Na interface causing another passivating interphase. This may result in a considerable electrical resistance, which then leads to an incorrect measurement of the cell voltage.

There are numerous studies, which report that HC capacities can be determined in 2032 coin cells in half-cell configuration. However, upon closer analysis most works lack in experimental details regarding the cell assembly, exact cycling conditions and/or raw data. In some cases, it becomes apparent that charging continued at negative potentials, so that plating of sodium is expected, thus questioning meaningfulness.

Overall, part A of the round robin study highlights that a three-electrode setup and voltage control by use of a reference electrode is essential for a reliable determination of the capacity of hard carbon and stands in agreement with our previous study.^[17]

NVP/C Half-Cells (RR-part B)

Key results of part B for the investigation of the NVP/C electrodes in a half-cell setup are shown in Figure 8. For the most accurate determination of the electrochemically available

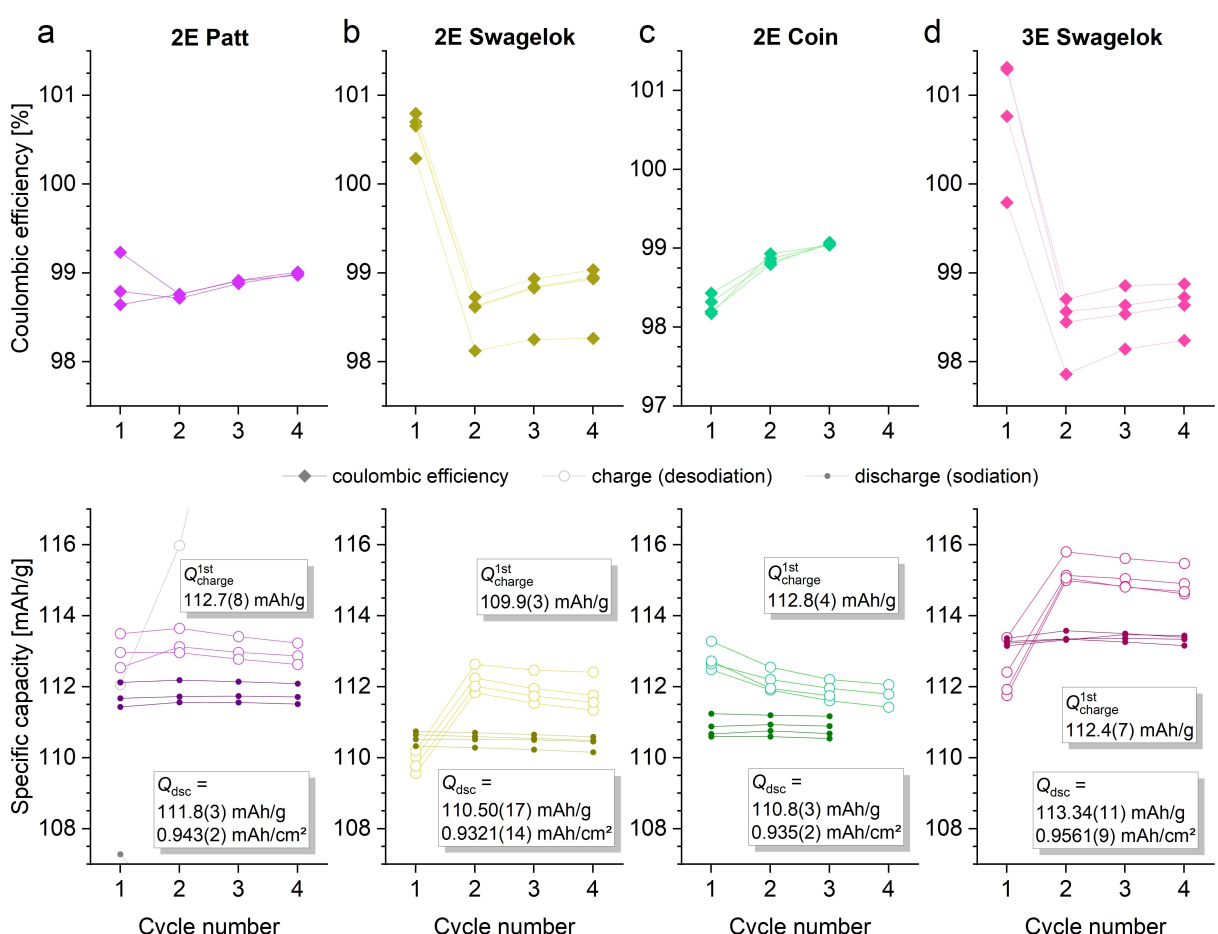


Figure 8. NVP/C vs. sodium half-cell formation results from four C/10 cycles: top panels display coulombic efficiency, while bottom panels visualize the specific capacity of each dis/charge cycle measured. Specific capacities refer to pure NVP.

sodium in the NVP/C cathode, which in theory allows for the best determination of the N/P ratio in full-cells, the charge capacity of the first cycle should be evaluated. In reality, however, parasitic side reactions (electrolyte decomposition on the reactive surface of sodium), which mainly occur during the first charging, lead to an overestimation of this value and thus to an overestimation of the electrochemically active sodium inventory within the cathode active material. As can be seen in Figure 8, the average values for the specific capacity of NVP determined from the first cycle charge capacity ($Q^{1\text{st}_{\text{charge}}}$) of the NVP/C electrodes range from 109.9 to 112.8 mAh/g for the 2E Swagelok cell and the coin cell, respectively.

The first cycle charge capacities for both 2E and 3E Swagelok-type cells are noticeably reduced by 2.0 to 2.5 mAh/g, compared to the subsequent cycles. The reason for this is not clear. In principle, such behaviour would be expected with a slightly Na-deficient active material, like e.g. $\text{Na}_{2.96}\text{V}_2(\text{PO}_4)_3$, but the results of the elemental analysis clearly contradict Na deficiency (see above and Table S1). Moreover, a corresponding reduction in first cycle charge capacity is not observed in 2E Patt cells (a) and 2E coin cells, (c). This rather indicates that the deviations of the first cycle charge capacity are a cell format-specific phenomenon and emphasises once more how important it is to bear in mind the possible influence of cell formats on test results.

A more robust approach of estimating the capacity of the NVP/C cathodes in half-cell configuration is to analyse the capacity during sodiation, that is, the discharge capacity. This is commonly done in high voltage LIB systems, which are even more susceptible to side reactions during initial charging.^[33] Here, all cell formats, yield highly reproducible values averaging between 110.5 to 113.3 mAh/g NVP (the exact numbers including the e.s.d. are noted in Figure 8). Considering the discharge capacity, all cells yielded reasonable results slightly below the theoretical capacity of 117.6 mAh/g. The experimental areal capacities for the different cell formats are in the range of 0.932 mAh/cm² (2E Swagelok cells) to 0.956 mAh/cm² (3E Swagelok cells), and thus are likewise very close to the theoretical value of 0.97 mAh/cm², which was calculated based on the electrode mass and NVP content (see above).

Some minor deviations occurred during testing: One Patt cell failed for unknown reasons. In case of the coin cells, a power outage occurred during the last discharge cycle, therefore, the last data point in discharge capacity and CE plot is missing. The Swagelok cells again show the highest reproducibility for part B of the round robin study, as can be seen from the diagrams and the lower standard deviations of the discharge capacity in Figure 8. The slightly higher discharge capacity in the 3-electrode Swagelok cell again might be due to better current control via the third electrode. The potential curves of all individual cells are shown in the Figure S2.

In summary, all four tested cell formats delivered reliable half-cell results for the capacity of the NVP/C electrode. Thus, it becomes obvious that the determination of specific capacities for cathode active materials ranging in potential windows of several volts (vs. Na/Na^+) is significantly less susceptible than the determination of the capacity of HC electrodes, where a

substantial part of the plateau including the cut-off potential for charging is close to zero volts (vs. Na/Na^+).

NVP/C vs. HC Full-Cells (RR-part C)

Finally, in part C of the round robin study, NVP/C vs. HC full-cells are investigated. Key results of the cell formation cycles at C/10 and subsequent continuous cycling at 0.5 C are shown in Figure 9 (see Figure S3 for potential curves) and Figure 10, respectively. The detailed cycling protocols are given in the experimental section.

All cells with two-electrode configuration provide highly reproducible and consistent results (cf. Figure 9a-d). The ICE values are in the range of 80.0% (2E Swagelok cell) to 82.9% (Patt-Cell) and the CE is above 99% in the subsequent formation cycles 2–4 (cf. CE^{2-4}). The first cycle charge capacities ($Q^{1\text{st}_{\text{charge}}}$), that is the capacity of the first desodiation of NVP/C, are in the range of 110.6 mAh/g (2032 coin cell) to 112.7 mAh/g (Patt cell). The 3E Swagelok cells likewise yield a very reliable initial charge capacity of 112.1 mAh/g and thus confirm the values found by half-cell measurements. The discharge capacities, however, in the three-electrode cells are noticeably reduced and scatter significantly. Note that we either had to use FEC-containing electrolyte, which was found to be suitable for half-cell experiments or use FEC-free electrolyte, which was shown previously to favour long-term performance. In light for better comparison of full-cell results, FEC-free electrolyte was used, and it can be assumed that the elemental sodium used as a reference electrode reacted with the FEC-free electrolyte, causing substantial side reactions.^[34] This issue could possibly be resolved by use of a different electrolyte or reference electrode,^[35] such as $\text{Na}_3\text{V}_2(\text{PO}_4)_3$.^[36]

Based on all four C/10 formation cycles of all four cells, the discharge capacities of the well-functioning cell formats 02 (a) to 04 (c) are in the range of 90.6 mAh/g to 94.8 mAh/g corresponding to the NVP active material. This may not be an impressive capacity for a battery material in general, but the values are higher than for previously reported NVP vs. HC based full-cells, where depending on the N/P ratio ~80 (N/P = 2.59)–90 (N/P = 1.05) mAh/g were achieved.^[24] When considering, that 87% ICE for HC can be reached (see experimental results above from 2E Swagelok cells) and by adjusting optimal balancing, theoretically specific capacities based on NVP active material of 98.3 mAh/g could be achieved in the full-cell with N/P = 1. The discharge capacity at 0.5 C and its retention over the first 100 full cycles is shown in Figure 10. During cycling, cells C_03-02 and C_04-02 experienced prolonged interruptions and finally the cell tests were aborted after 69 and 95 cycles, probably due to a malfunction or improper handling of the potentiostat; the corresponding cell tests are shown in grey.

In general, cell formats 02–04 (a)-(d), which are based on a two-electrode configuration, show very reasonable and reproducible results in the cycling stability test. The individual values of the discharge capacity retention after 100 cycles are also listed in Figure 10. Evaluation of the three best cells indicate, that overall, 2032 coin cells perform most stable. The cells show

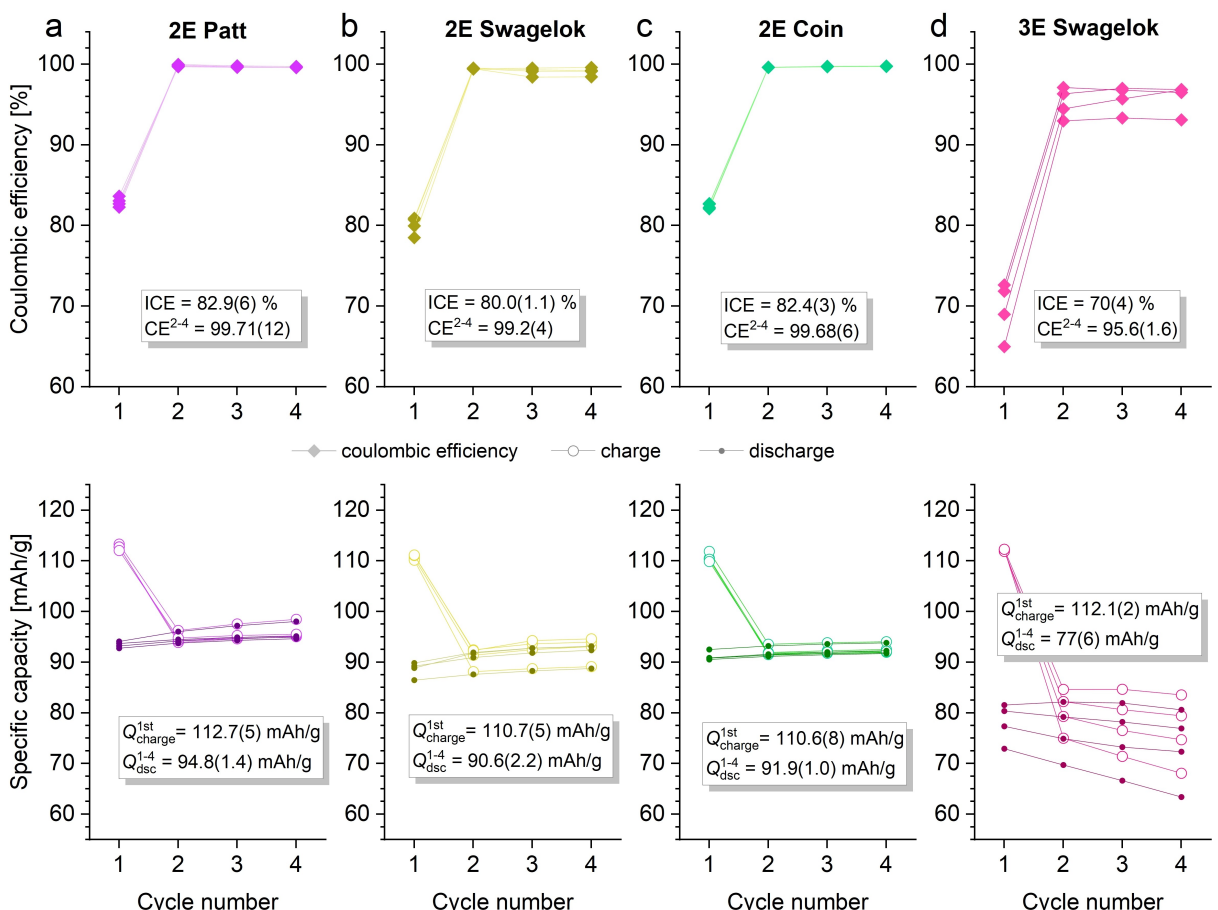


Figure 9. NVP/C vs. HC full-cell formation results from four C/10 cycles: top panels display coulombic efficiency, while bottom panels visualize the specific capacity referred to pure NVP of each dis/charge cycle measured.

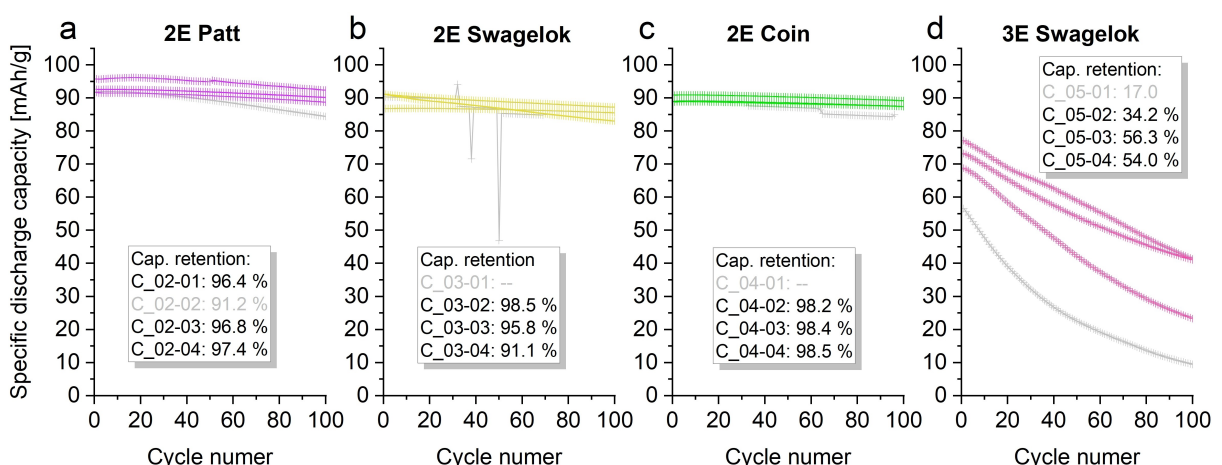


Figure 10. NVP/C vs. HC full-cell specific discharge capacities referred to NVP during continuous cycling at C/2 dis/charge rate.

a very uniform ageing behaviour and the values for the 100 cycles capacity retention are in the narrow range of 98.2–98.5%, which means that the capacity retention per cycle is > 99.98%. This is consistent with findings from previous studies, where it was shown that NMC111 vs. Gr LIB cells show > 1500

full cycles before an (arbitrary) end of life is reached at 80% of the starting capacity.^[16]

Overall Results

The results from parts A, B and C of the ring study once again clearly show that preparation of cells, the cell formats used, and configuration/testing mode can have a considerable influence on the results of battery cell tests. It is also clear that none of the cell formats tested herein can handle all tasks solely. Overall, two critical aspects need to find attention: Careful cell setup and measurement technique with voltage control over a reference electrode need to be applied when determining accurately the specific capacity of HC in half-cell configuration (see part A). In case of full-cell characterisation, low ICEs and low long-term cycling stability are obtained when three-electrode setups are used (see part C).

For a visual overview of the strengths and weaknesses of the individual cell types, spider charts are shown in Figure 11.

Each category evaluated in the spider chart ranges from 0–4 (with 4 representing the highest (best) achievable score) and categories are defined as the following: 1) Functionality, correlating to the number of cells that were classified as “yielding meaningful measurement data”. 2) Reproducibility, evaluating the number of cells that delivered repeatable results. 3) Accuracy, representing how well the collected data correspond to the expected value, e.g. specific capacity of HC (functional cells only). 4) For half-cell setups, the experimental effort is evaluated considering both, manufacturing skills and instrumental effort. For the full-cell setup, the cycling stability is evaluated by means of reproducibility of following measurement cycles. 5) Suitability, considering if the cell format is adequate for the measurement.

It was shown previously, that the capacity of hard carbon as anode active material for sodium-ion batteries can be determined reliably using three-electrode Swagelok cells.^[17] For the hard carbon electrode investigated herein, the setup likewise yields the best results. Coin cells, Patt cells and 2E Swagelok cells are very well suited for half-cell measurements of cathode active materials and for full-cell measurements. From RR part C, coin cells appear to be the cell format achieving the highest long-term stability.

Since the Patt cells can also be built in a three-electrode configuration using a suitable reference electrode (which was not possible due to the initial lack of reference electrodes), this format has the potential to overcome both critical challenges, correct measurement of hard carbon in the half-cell setup, as well as long-term stable full-cells. The disadvantage of the Patt cells is, due to the expensive cell housings, that it is rarely possible to build 10 or more cells in parallel, and it will hardly be possible to test many cells over long periods of time.

The 2E Swagelok cells were the only cell format using a two-electrode configuration to achieve an approximately correct determination of the hard carbon capacity. Overall, the two-electrode Swagelok-cells prove a highly versatile and reliable cell format. Nevertheless, the ring study part A confirms that according to the current state of knowledge,^[17] a three-electrode configuration is necessary for the correct capacitance determination of hard carbon electrodes, and thus the latter is only achieved with the 3E Swagelok cell. This cell format likely shows excellent results for the determination of positive electrodes in half-cell configuration. However, a clear disadvan-

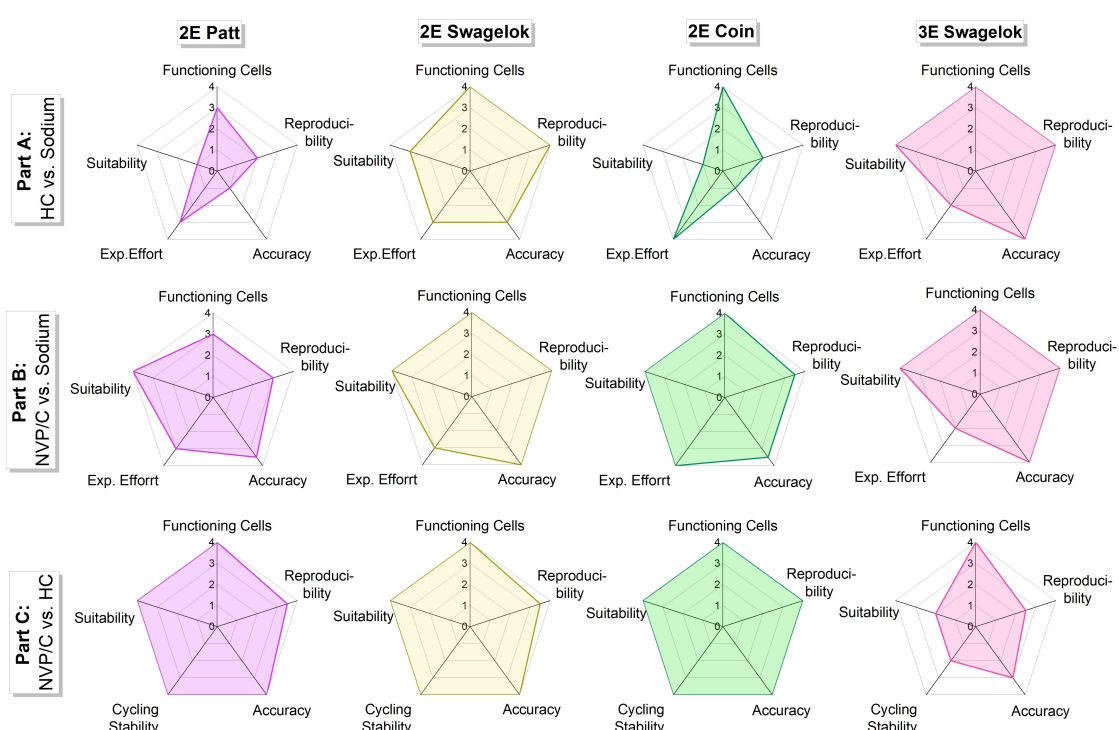


Figure 11. Spider charts comparing different categories (functionality of cell, reproducibility, accuracy, experimental effort (only for half-cells)/cycling stability (only for full-cells), suitability) of the individual cell formats used for NVP/C, HC half-cell, and NVP/C/HC full-cell measurements.

age is that the cells with reference electrodes seem to degrade quickly and capacity retentions in full-cells are underestimated.

The round robin study highlights that redundancy and transparent reporting of measurement conditions and raw data is a crucial, but unfortunately often neglected aspects of good scientific practice. As a compromise between limited resources on the one hand, and reliability of the results on the other, at least three cells per experiment should be tested and only reported if reproduced including statistics. Even with high-quality and well-maintained hardware, failures of individual tests can hardly be avoided, but reproducibility must be ensured.

Pilot Scale NVP/C vs. HC Full-Cells

In order to bridge the gap from research-type results to industrial application relevant data, and to obtain relevant KPIs, single- and multi-layer pouch cells were constructed for the last part of the work. Photographs of the NVP/C vs. HC pouch cells are shown in Figure 12. Details of the cell assembly can be found in the experimental section and a previous study.^[18] Although it is common that industrial-type battery cells contain an anode overhang (which guarantees the cathode to always be aligned facing sufficient counter-anode area), we probed to minimise initial irreversible loss of sodium inventory on hard carbon by omitting overhang area. Thus, each three cells of two different types of single-layer pouch cells were built: In accordance with the full-cell coin cell setup (2E coin), single-layer pouch cells (SLP-1:1) were built without overhang of the anode. Also, cells were built with a circumferential anode overhang of 2 mm resulting in a ratio of the anode:cathode area of 1.16:1 (SLP-1.16:1). Finally, but in this case due to the lack of sufficient high amounts of active material (and thus electrodes) only a single multi-layer pouch demonstrator (MLP-1.05:1) cell containing 16 cathode and 16 anode sheets (single-sided coated) was assembled. Herein, the anode and cathode footprints are 3.9×21.2 cm and 13.5×20.8 cm, respectively, yielding an anode:cathode area ratio of 1.05:1 and circumferential anode overhang of 2 mm.

Key results of the formation cycles are shown in Figure 13 (see Figure S4 for voltage profiles), together with the results of the coin cells from the round robin studies (see above) because this cell type generated the best results in research-type format. Specifications for the cell setup are summarised in Table 3 for comparison. It becomes obvious that all cells, in principle, yield in similar capacities for charge/discharge and coulombic efficiencies.

In the SLP-1.16:1 cells, nearly the same specific charge capacity is found (111 mAh/g) as obtained from 2E coin cells. However, the discharge capacity and thus the initial coulombic efficiency is significantly reduced compared to the coin cells and SLP-1:1 cells. The reason for the reduction of the discharge capacity is most likely due the anode oversize, leading to additional irreversible loss of sodium-ions. The SLP-1:1 yield almost the same discharge capacity as the coin cells, however, significantly higher charge capacities during the first cycle and an additional bump in the voltage profiles (Figure S4a) indicate parasitic side reactions, which is why we do not generally recommend omitting the anode oversize. Moreover, the CE values of the subsequent cycles vary considerably (see Figure 14). Considering the discharge capacities from the formation cycles, the MLP cell data matches the one of 2E coin cell and SLP-1.16:1 cells. This great reproducibility allows us to assume that reasonable data is obtained from the one MLP cell. The specific capacity based on NVP active material, relative discharge capacity, and the CE of the full-cells during continuous cycling at 0.5 CCCV/0.5 C is shown in Figure 14a-c respectively. In all cell formats, a similar and moderate capacity loss is observed and the corresponding capacity retentions are in the range of 97.5 to 98.7% over the first 100 cycles. As listed in Table 3, normalized to the cathode surface, the initial discharge capacity at C/2 varies between 0.68 mAh/cm² to 0.80 mAh/cm² in the cells and cell types. These variations are mainly due to two reasons: the reduced capacity in the SLP-1.16:1 cells originates from the large anode oversize and thus higher initial sodium-ion losses as discussed above for the formation. The higher areal capacity in the coin cells results from variations of the material loading in the corresponding cathode sheets. As shown in Table 3, in the coin cells, the electrodes contained on average, ~10.0 mg/cm² active material,

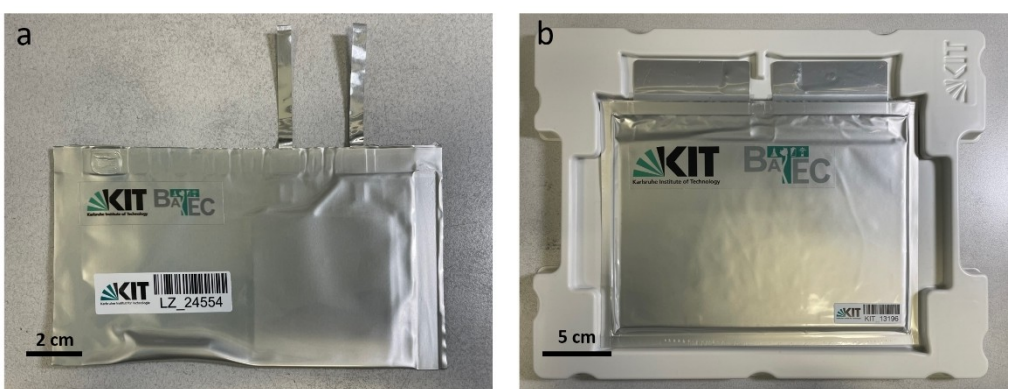


Figure 12. Photos of pilot scale NVP/C vs. HC pouch cells. a) 19 mAh single-layer electrode pouch cell (SLP). b) 3.5 Ah multi-layer (16 cathodes/anodes) electrode pouch cell (MLP).

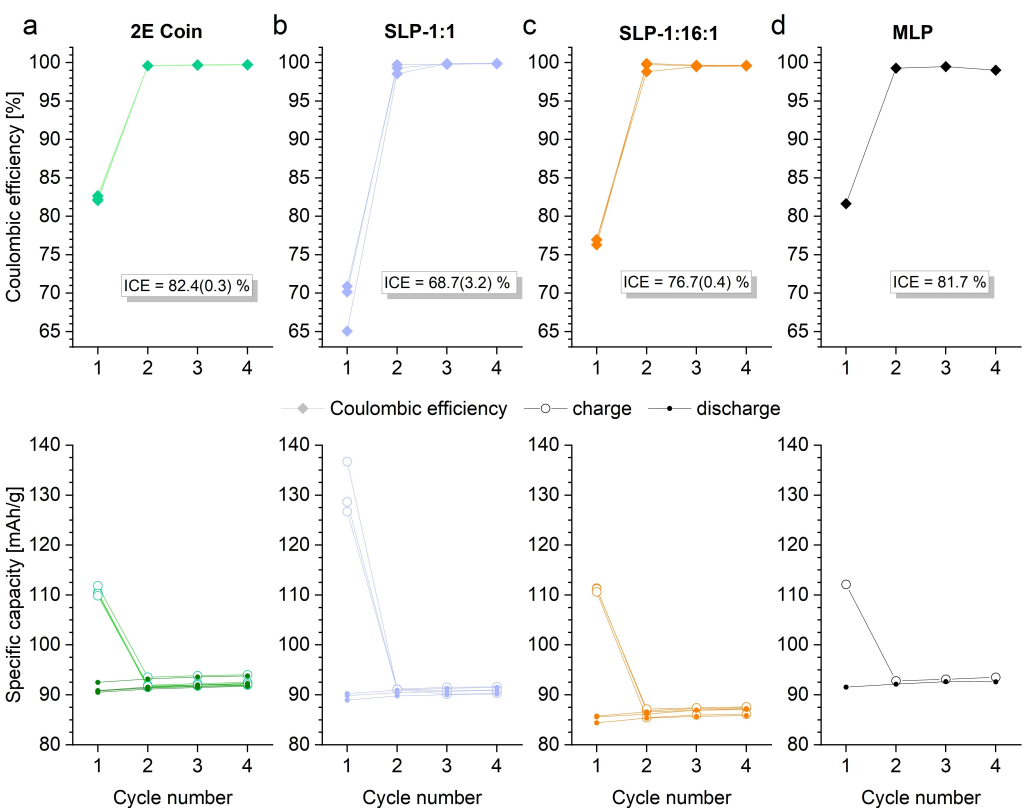


Figure 13. NVP/C vs. HC full-cell formation results from four C/10 cycles: top panels display coulombic efficiency, while bottom panels visualize the specific capacity referred to pure NVP of each dis/charge cycle measured. a) 2E coin cell, b) SLP-1:1, c) SLP-1.16:1 and d) demonstrator MLP-1.05:1. Ratio refers to anode:cathode area.

Table 3. Comparison of cell composition and resulting capacities of 2E coin, SLP-1:1, SLP-1.16:1 and MLP. Note that the loading of the cathode used for coin cells are higher than for pouch cells.

Cell type		2E coin	SLP-1:1	SLP-1.16:1	MLP-1.05:1
Cathode surface	[cm ²]	2.01	24.86	24.86	4490.60
Anode : cathode area ratio		1:1	1:1	1.16:1	1.05:1
Electrolyte volume of the cell	[μL]	110	450	450	57000
Electrolyte : NVP ratio	[μL/cm ²]	54.7	18.1	18.1	12.7
Electrolyte : total capacity ratio	[mL/Ah]	66.2	23.4	25.1	16.1
Active material	NVP/C	[mg/cm ²]	10.0(3)	9.51(8)	9.37(17)
	pure NVP	[mg/cm ²]	8.9(3)	8.44(7)	8.32(16)
Discharge Cap	C/10 (4 th cycle)	[mAh/cm ²]	0.827(18)	0.772(16)	0.721(7)
		[mAh/g]	92.4(9)	90.9(7)	86.7(8)
		[mAh]	1.66(4)	19.2(4)	17.9(2)
Discharge Cap	C/2 (1 st cycle)	[mAh/cm ²]	0.797(11)	0.739(17)	0.680(7)
	C/2 (100 th cycle)	[mAh/cm ²]	0.787(8)	0.727(17)	0.667(11)
100 cycles capacity retention	[%]	98.7	98.3	98.1	97.5

whereas cathodes used for fabrication of the pouch cells contained only ~9.5 mg/cm². Thus, the 5% increase of active material loading give a reasonable explanation for somewhat higher discharge capacities. The MLP was the only cell that was not tested in a climate chamber, but in an air-conditioned room. Due to the somewhat stronger pronounced temperature

fluctuations in the day-night cycle, a typical variation of the discharge capacity can be seen especially from cycle 40 to 80.

The CE values of the different pouch cells (and 2032 coin cells, for comparison) are shown in Figure 14c. The coin cells and SLP-1:16:1 pouch cells show a steady cycling behaviour and CE values >99.9% after 20 cycles. The CE values of the SLP-1:1 cells in contrast considerably vary from cycle to cycle

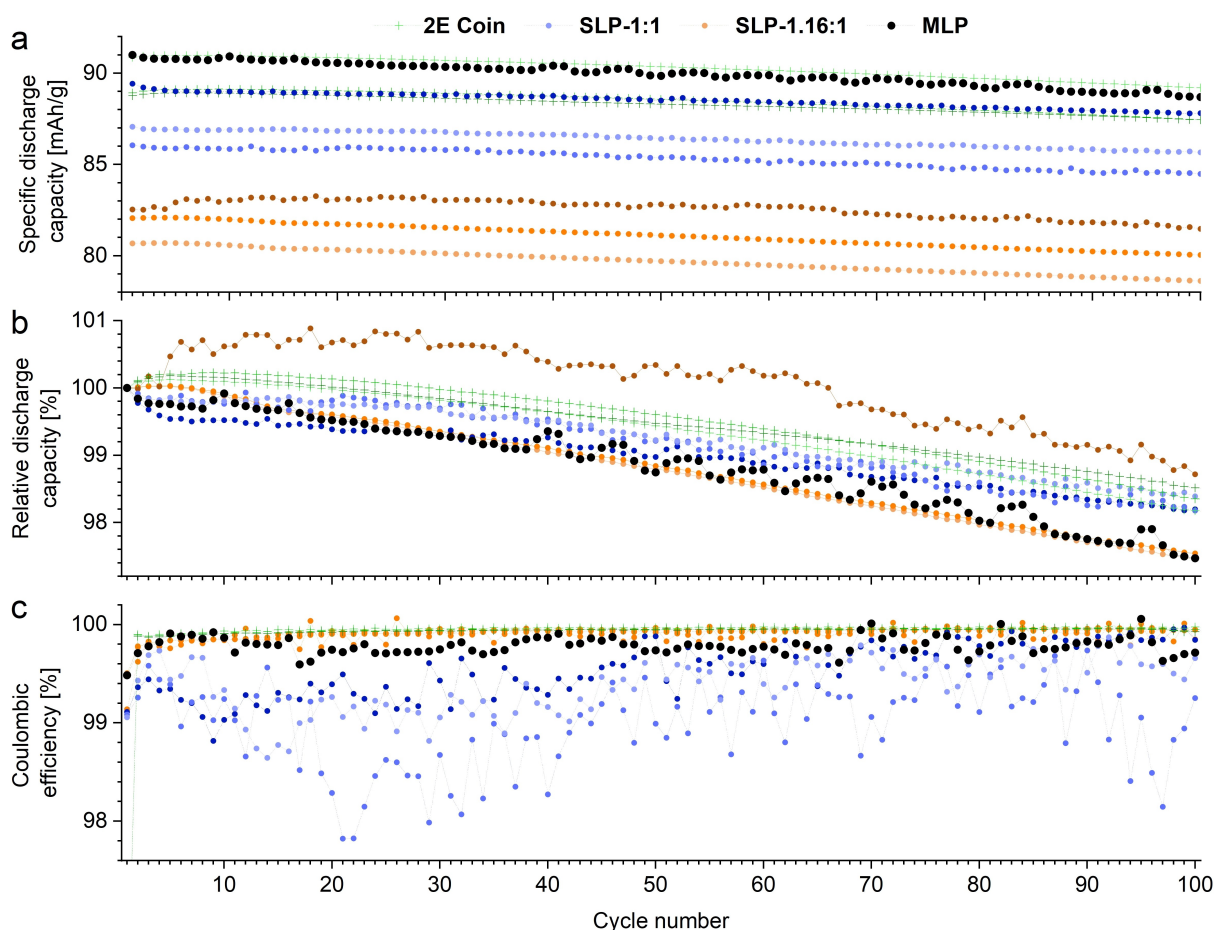


Figure 14. NVP/C vs. HC full-cell continuous cycling data over 100 cycles showing a) specific discharge capacities based on NVP active material mass, b) relative discharge capacities, c) coulombic efficiencies.

and are significantly reduced with an average value of 99.3%. This indicates that the missing anode overhang might lead to additional side reactions, which however, do not seem to affect the sodium inventory and thus discharge capacity of the cells. Such effects could be reversible sodium plating at the anode edges. The average CE values of the MLP are 99.78%, and range between 99.48% to 100.05%. Overall, the MLP with an overhang area of 5% shows very close specific capacities (~90 mAh/g) and CE values, as well as capacity retention over 100 cycles to the 2032 coin cell. Up to that point in ageing, dry up of electrolyte seems not to be an issue based on the MLP data obtained (note that MLP only has $\frac{1}{4}$ of the electrolyte: capacity ratio compared to the 2E coin cell). Since the MLP also shows no elevated temperature behaviour during cycling, it might be expected that 2032 coin cell data can project cycling behaviour at low C-rates, here C/2, of the MLP. The greatly oversized anode (16%) for SLP-1.16:1 causes a dramatic decrease in overall specific capacity to ~77% with respect to the first formation cycle and starting values of ~82 mAh/g during cycling. It should be noted, that by calculation the initial loss does not translate to a proportional irreversible loss of sodium-ion inventory, meaning that not all of the overhang area is actually electrochemically active. Having zero overhang SLP-1:1 obviously shows larger specific capacities than SLP-1.16:1, but

unlike for the 2032 coin cell it is extremely difficult to perfectly place the cathode over the anode without some misalignment. The above-mentioned issues most likely are a result of that fact.

In order to gain a realistic impression of the practical discharge capacity at higher C-rates and the associated heat generation, which is only accessible in large-format NVP/C vs. HC cells, the MLP was further characterised in a rate capability test, which was conducted after the cycle stability test. To avoid the risk of sodium plating on the anode, the charge rate of 0.5 C with a CV-step to 0.05 C was retained. During the rate capability test, the discharge rate was increased up to 20 C and all C-rates were performed twice (for clarity only one set of data for each C-rate is shown, however, no differences were observed between two equal discharge rates). The individual currents were calculated based on the discharge capacity obtained during the cell formation, that is, 1 C = 3.54 A. Interestingly, the first 0.5 C discharge step from the rate capability test yielded a cell and specific capacity of 3.375 Ah, or 89.91 mAh/g, respectively, which is slightly above the 3.350 Ah or 88.7 mAh/g of the last cycle of the cycling stability test. Such a partial recovery of lost capacity due to slow charge/discharge cycles (here C/10) is not unusual and is also characteristic of the NVP/C vs. HC system.^[16] The detailed results of the rate capability test are listed in Table S3, the corresponding voltage

profiles are shown in Figure 15b. It becomes obvious, that up to 15 C, the voltage of the discharge plateau gradually decreases from 3.21 V at 0.5 C to 2.42 V at 15 C and the discharge capacity is reduced from 89.9 mAh/g to 61.6 mAh/g. Even at 15 C only moderate heating of the cell to 40.5 °C was observed (see Figure 15a), which increased to 40.7 °C in the following pause. At a discharge rate of 20 C, the cell voltage dropped immediately below the lower voltage limit of 2.3 V due to immense over-potential and no noteworthy discharge capacity can be accessed within the voltage window of 2.3 to 3.9 V. No signs of cell damage caused by the rate capability test could be found, as the initial capacity was reached almost undiminished in the final 0.5 C cycles.

Finally, based on the total weight of MLP (234 g) and data obtained from the rate capability test, for each C-rate the mean discharge voltage and the corresponding total capacity of each discharge step was used to generate a Ragone plot, as can be seen in Figure 15c. The first set of data (per cell weight, 234 g, dataset A) resulted from the calculations described above. The overall energy density is rather low with ~45 Wh/kg "Real cell: MLP-1.05:1, dataset A" and provides on average a power density of ~24 W/kg at C/2 discharge rate. At 15 C the power density increases to 550 W/kg providing 24 Wh/kg energy density. Based on the footprint of the separator and height of the cell stack ~100 Wh/L are achieved at C/2. These performance numbers could be somewhat improved for our particular cell design. For once, most likely excessive electrolyte amount is present within the cell, which can be further reduced. Secondly, the overall loading of the electrodes can be increased, however, this might also increase resistance, thus increase the overpotential and worsen the thermal behaviour.

Furthermore, as stated above, single-sided coated electrodes were used for the assembly of the MLP. If double-sided coated electrodes were used, one could subtract half of the

total mass of the current collectors. This would result in performance data indicated by "Double-side coating, dataset B", with energy densities of ~50 Wh/kg and power densities of ~27 W/kg for C/2.

Taking into account that excess electrolyte, too thick separators and at least for the anode too thick aluminium current collectors were used, the energy and power density easily can be increased on cell level. More precisely, only 43 mL (=12 mL/Ah) of electrolyte instead of 56 mL can be used (if half of the separator thickness is considered as state of the art, namely 14 µm (40% porosity) instead of 28 µm and if any excess electrolyte volume is eliminated) and also 15 µm thick current collectors (4.12 mg/cm^2) could be used for cathodes and anodes, also considering double-sided coating. In that case referring to the dataset "C: Electrodes and electrolyte", but also excluding any packaging material and tabs a cell weight of 145 g could be achieved, which would yield in 73 Wh/kg at C/2 with an average power density of 39 W/kg increasing to ~890 W/kg at 15 C. Herein, ~120 Wh/L on stack level are achieved. According to calculations from literature, a theoretical value of 73 Wh/kg is reported for the NVP/HC full-cell based on electrodes with only half of our mass loading, N/P ratio of 1.05, but probably too small amounts of electrolyte (3.7 mL/Ah).^[24]

Another set of data can be obtained only considering the actual electrode coating. This data (E: Electrode coating only) set might be useful when comparing different cell build ups, e.g. round cell, prismatic vs. pouch, as their inactive components add to a different degree as passive mass to the total weight. In that case, ~160 Wh/kg are obtained in our measurements at C/2 on electrode coating basis with a power density of 86 W/kg, increasing to 1930 W/kg at 15 C (still delivering 85 Wh/kg).

If one only referred to the active materials including both NVP and HC (trace F: Active material only) 173 Wh/kg will result

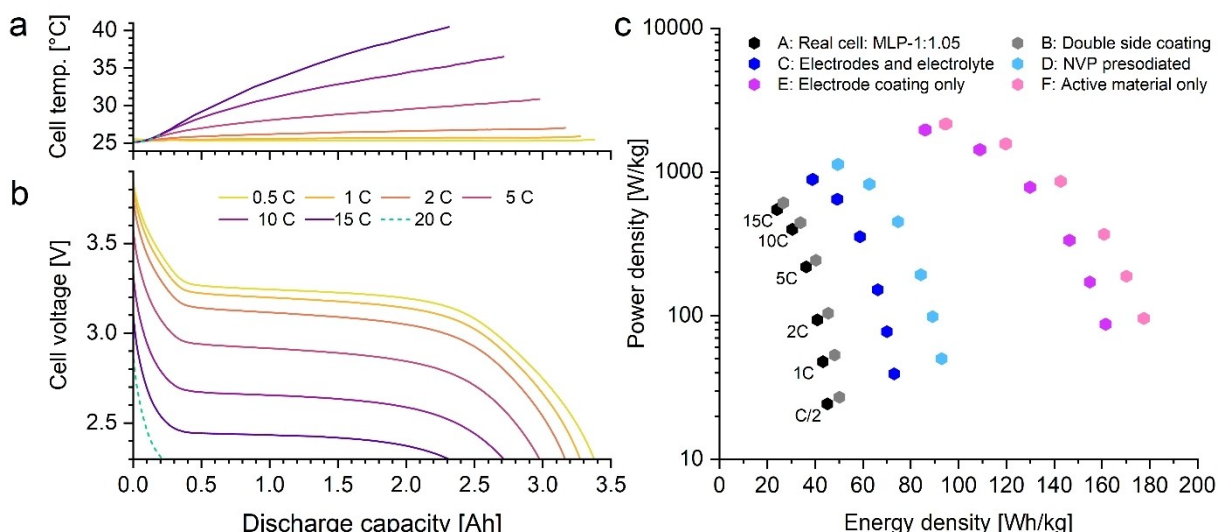


Figure 15. Temperature behaviour (a) and voltage profile (b) during the rate capability test of the MLP demonstrator using C/2 CCCV for charging and varying C-rate (C/2 to 20 C, back to C/2) for discharge. (c) Ragone plot showing average discharge power density capability with corresponding energy density of the MLP-1.05:1 demonstrator (per real total cell weight, trace A). When omitting further inactive components of the cells other data sets (traces B, C, D, E, F) were generated.

at C/2 (delivering 95 W/kg) and at 15 C still 92 Wh/kg are obtained with average ~2130 W/kg power density. These numbers, especially the latter ones, are supposed to show, which dramatic differences in KPIs are obtained, when data is only reported on material level and its energy or power density is directly projected to energy and power density omitting any inactive components. Even worse, some highly promoted works report on KPIs, which are solely based on the anode or cathode active material level.

Finally, based on the cell data practically collected, we present an outlook for the potential energy density of the NVP/C vs. HC full-cell stack including electrolyte (scenario C), but considering 1:1 balancing and pre-sodiation of the active material to max out capacities of the cathode and anode. In that case (dataset D) energy densities of 93 Wh/kg (with ~120 Wh/L) can be achieved providing 50 W/kg at C/2. These results stand in contrast with calculations based on LIB models concluding energy densities of 105 Wh/kg at similar electrode loading but even greater N/P ratios of 2, thus questioning the stated achievable 150 Wh/kg when NVP loading is increased to >19 mg/cm².^[24]

Conclusions

- (1) In order to facilitate research on sodium-ion batteries, and to allow for better comparability, reference materials in the form of powders, electrodes and electrolytes were defined, prepared, distributed and carefully characterised as part of this study.
- (2) The development of high energy density SIB full-cell requires careful consideration of the balancing, as ~20% of sodium-ion inventory is lost irreversibly during formation. Therefore, an accurate capacity determination of the hard carbon anode and a respective cathode active material is necessary.
- (3) Particularly, the accurate determination of the specific capacity of hard carbon remains challenging, because of the potential plateau and lower potential cut-off being close to zero volts (vs. Na/Na⁺). Our findings suggest the use of voltage controlled three-electrode cell setups as necessary to obtain meaningful and reproducible data.
- (4) Although a variety of different research-type battery cell constructions are used and reported in literature, it becomes obvious that each cell type (2/3-electrode) and/or construction has its specific purpose and is to be used for particular measurements, e.g. impedance, long-term testing, etc.
- (5) Simple 2032 coin cells can project long-term cycling stability of full-cells, if the C-rate is rather low and if thermal effects can be neglected. However, any dry-up effect of electrolyte is potentially masked as coin cells are rather flooded with electrolyte.
- (6) In general, electrochemical experiments should be at least duplicated and raw data needs to be provided to allow for first-hand evaluation and checking.

- (7) Overhang area significantly reduces the capacities by irreversible loss of the sodium-ion inventory, but not proportionally to the overhang area.
- (8) NVP/C vs. HC full-cells on stack level will deliver under optimised conditions, such as close balancing and including pre-sodiation strategies, ~90–100 Wh/kg.

Experimental

NVP/C Active Material Preparation

The NVP/C active material was synthesised starting from Na₂CO₃, NH₄H₂PO₄, NH₄VO₃ and β-Lactose following a protocol described in detail previously.^[16] To avoid repetition, the points that deviate from this previous report are covered herein. According to the molar ratio of 1:2:1.3:0.7, 1274 g of the starting materials were dissolved in 12 L of deionised water and then spray dried. This synthesis was then repeated three times yielding roughly 4 L of precursor powder. The first calcination was carried out as described previously,^[33] using the furnace CWF12/65 (Carbolite, Gero). A total of 2800 g of precursor material was obtained in 6 oven runs. Each 700 g precursor material was diluted with 4 L of deionized water, ground with 0.2 mm zirconia grinding balls for 6.5 h. Afterwards, 7 g Poly(acrylic acid) (PAA), 63 g Poly(ethylene glycol) PEG and 2.5 L deionised water were added and the suspension was spray dried again. This step was repeated three times. The powder obtained was split up and calcined in three consecutive oven runs under Ar/H₂-atmosphere (3% H₂) at 800 °C for 5 h yielding 2500 g of the NVP/C active material. Supplier and quality of all chemicals needed are listed in Table 4.

NVP/C and HC Electrode Preparation

The NVP/C cathode was prepared in an NMP-based process. The NVP/C powder was dried over night at 120 °C prior to the slurry preparation. The slurry was then mixed in a dissolver stirrer (Dispermat SN-10, VMA Getzmann), where carbon black and graphite, a Poly(vinylidene fluoride) (PVDF) binder-solvent solution with 7.5 wt% and about 50% of the required amount of NMP were dispersed. The NVP/C composite material and remaining NMP were added to the dispersed PVDF/NMP and conductive additive slurry to adjust the solid content to 50 wt%. Vacuum was applied to remove existing gases from the slurry. It was then coated onto an aluminium foil with a thickness of 16 μm by a doctor blade at a line speed of 0.15 m/min and dried in line at 80 and 100 °C in two

Table 4. Overview of the chemicals used for NVP/C synthesis including supplier and quality.

Component	Supplier	Quality
Na ₂ CO ₃	VWR Life Science	anhydrous
NH ₄ H ₂ PO ₄	VWR Chemicals	
NH ₄ VO ₃	Thermo Scientific	
β-Lactose (<30% α-anomer basis)	Sigma-Aldrich	≥99% total lactose basis
Poly(acrylic acid) (PAA)	Sigma-Aldrich	
Poly(ethylene glycol) 400 (PEG)	Merck	

Table 5. Composition of the NVP/C electrode and hard carbon electrode.

Component	Source/trademark	Content
Composition of the NVP/C Electrode		
NVP/C	own synthesis	90.5 wt%
Carbon black	TIMCAL C-NERGY Super C65 (Imerys)	3.0 wt%
Graphite	KS6 L (Timcal-Imerys)	2.0 wt%
PVDF	Solef 5130 (Solvay)	4.5 wt%
Composition of the hard carbon Electrode		
Hard carbon	Kuraray Kuranode Type II (9 µm)	93.0 wt%
Carbon black	TIMCAL C-NERGY Super C65 (Imerys)	1.4 wt%
Carboxymethyl cellulose (CMC)	MAC500LC (Nippon Paper)	1.9 wt%
Styrene-butadiene rubber (SRB)	BM-4xx (Zeon)	3.7 wt%

consecutive drying chambers under circulating air using a role-to-role coating line (KTF-S, Mathis AG). The width of the coating and aluminium foil was 145 and 200 mm, respectively. The final composition of the cathode, including the source of the used chemicals is listed in Table 5. Graphite is added primarily due to its beneficial effect during calendering. It acts as a dry lubricant, and electrode porosity reduction is achieved with fewer cracks of the secondary particles.

Commercial hard carbon material KURANODE™ Type II from KURARAY CO., LTD was used as the active material in the anode. The preparation of a water-based slurry was conducted in accordance with the detailed procedure described in a previous study.^[4,5] The slurry did not exhibit any agglomerates. The final solid content of the slurry was 43 wt%. The individual anode components, including the source of the chemicals in the dried anode, are likewise listed in Table 5. The electrodes were manufactured in a continuous process on a roll-to-roll machine (Coatema Coating Machinery GmbH). The specified composition was chosen based on the experience of previous studies on the drying behaviour of the hard carbon slurry and electrodes and the aqueous binder system CMC/SBR.^[4,5] The width of the coating applied on aluminium foil by the slot-die was 15 cm. The production speed was 0.5 m/min. The coating underwent two impingement drying sections, with a temperature of 110 °C in each instance. Both electrodes were then calendered at a roller temperature of 50 °C (GKL400, Saueressig, Germany) with a rolling speed of 1 m/min.

Material and Electrode Characterisation

The particle morphology of NVP/C active material and cross-sections of the calendered electrodes were studied by scanning electron microscopy (SEM) with a Supra 55 FE-SEM (Zeiss) using acceleration voltages of 2–10 kV, respectively. Cross-sections were prepared by an ion-milling process using argon-ions (TIC-3X, Leica Microsystems). The carbon content of the NVP/C powder was measured via a CS-analyser (Inductar CS cube, Elementar). The composition of NVP/C was further investigated by elemental analysis. Therefore, the sample was dissolved with acid in a graphite furnace. Subsequently, the elements except C and O were analysed by inductively coupled plasma optical emission spectrometry (ICP-OES). O was determined by thermal extraction with carrier gas (TGHE). X-ray powder diffraction data was collected on a Bruker D2 Phaser benchtop diffractometer (30 kV, 10 mA) with a Lynxeye XE-T detector using Cu-K α radiation in Bragg-Brentano geometry. The powdered samples were dispersed with isopropanol and were evenly spread over a zero-background Si sample holder, which

yields in a thin homogeneous layer. Data was collected over an angular range between 12 and 100° 2 θ using a step size and time per step of 0.02° and 4 s, respectively. The density of NVP/C was measured by means of He-pycnometry (Porotec pycnomatoc-ATC) using a sample mass of 0.60 g. The particle size distribution of the NVP/C active material was determined by a laser scattering particle size distribution analyser LA-950 (Horiba). The device's internal ultrasonic dispersion was used to dissolve agglomerates prior to the measurement. The granule porosity and pore size distribution of NVP/C was measured by mercury intrusion porosimetry with a CEI Pascal 1.05, Thermo Electron. The internal porosity P was calculated according to $P = V_p / (V_p + 1/\rho)$, where V_p is the inner specific pore volume, between 4 nm and 300 nm and ρ is the density of NVP/C. Nitrogen physical adsorption isotherms were measured with a surface area analyser Gemini VII 2390 (Micromeritics). Calculations of the specific surface were performed according to the Brunauer–Emmett–Teller (BET) theory. Prior to the measurement, specimen and tube were dried under vacuum at 120 °C for at least 16 h.

Electrolyte Preparation

Electrolytes were freshly prepared in an Ar-filled Glovebox (O_2 and $H_2O < 1$ ppm) from the components listed in Table 6. For the preparation, aluminium containers (Leicht&Appel) and volumetric flasks (Poly(propylene)) were used and after mixing, the electrolytes were transferred to aluminium vials (Leicht&Appel). The well-closed bottles were then airtight sealed in aluminium foil inside the glovebox and then stored at a temperature of 7 °C. The water content of the electrolyte was determined by means of Karl-Fischer titration using a C30 Coulometer (Mettler Toledo) to be less than 10 ppm.

Table 6. Electrolyte components used for the electrolyte preparation.
*Purities based on the manufacturers' specifications.

Component	Supplier	purity*
Ethylene carbonate (EC)	Gotion	> 99.5 %
Propylene carbonate (PC)	Gotion	> 99.5 %
Fluoroethylene carbonate (FEC)	Gotion	> 99.5 %
NaPF ₆	Chemfish	99.9 %

Round Robin Laboratory Research Cell Formats

All cells for the round robin study were assembled in Ar-filled gloveboxes with O₂ and H₂O levels < 1 ppm. The cells were built in different labs, but cycled at the same testing rig (details see below). NVP/C and HC electrodes from the same sheet were used. Electrolytes originated from the same batch. The type of separator installed, the preparation of the sodium counter and reference electrodes and the drying conditions of the separators and NVP/C and HC electrodes varied from lab to lab.

Cells from EL-CELL (PAT PRESS) were constructed as described by EL-CELL in two-electrode configuration. The cells and the corresponding cell parts (spacers, insets, etc.) were heated at 80°C in vacuum for 12 h and transferred into a glovebox. Separators (QMA, diameter of 22 mm) and cell material was dried inside of the glovebox at 120°C under vacuum. Commercial sodium disks from PI-KEM (UK) were used for the half-cell tests. Here, sodium is laminated onto an aluminium foil and both sides are protected with a plastic foil. After removing the foil, the disks were used directly for the cell tests.

Two-electrode Swagelok cells comprise a top and bottom tube manufactured from stainless steel 316Ti. The electrodes were dried at 120°C under vacuum. Glass fibre separators (Whatman GF/B) and metal cell parts were dried at 100°C, but remained within the glovebox for a longer period of time prior to cell assembly. For the preparation of the half-cells, sodium metal was rolled directly onto the Ni-metal current collectors with a diameter of 11 mm, in order to ensure low contact resistance between the sodium and the current collector and to prevent the electrolyte from penetrating into the interstitial space. Subsequently, each cell was filled with 0.1 mL of electrolyte. A stainless steel spring was used between the current collector and the top tube to maintain a constant stack pressure.

For the coin cells, based on previous experience,^[18] cell parts made of SUS316 L stainless steel of type 2032 housing (Hohsen, Japan), QMA glass fibre separator and a single spacer with a thickness of 1 mm were used. Electrodes were dried at 130°C in a heating vacuum chamber attached to the glovebox. For the half-cells, commercial sodium discs from PI-KEM were used, as described above.

Three-electrode Swagelok cells with a sodium reference electrode were assembled following the protocol of Müller,^[17] with the

exception that herein, a 12 mm sodium counter electrode was used. Metal parts of the Swagelok cells are made of S316 L stainless steel. Separators and electrodes were dried in a B-585 glass oven (Büchi) at reduced pressure at 140°C and 120°C, respectively.

An overview of the cell layouts and assembly of the cells is listed in Table 7.

Pilot Scale Cell Formats

Single-layer (SLPs) and multi-layer pouch cells (MLP), see photos in Figure 12, were manufactured in a dry room with a dew point of -60°C. The cell formats and assembly process have been described in detail previously.^[18] For the SLP-1:1 a cathode/anode footprint of 5.0×5.0 cm resulting in an area ratio of 1:1 were constructed. Using our standard pouch cell setup (SLP-1.16:1), a cathode and anode footprint of 5.0×5.0 and 5.4×5.4 cm, respectively, was used. The cathodes of the single- and multi-layer pouch cells have a footprint of 5×5 cm and 13.5×20.8 cm, respectively. Due to the lack of double-sided coated electrode material, the single-sided coated electrodes were used. In the large format multi-layer cell MLP, cathodes and anodes were assembled back to back in pairs, with exception of the outer anodes. In total, the multi-layer cell stack consisted of 16 cathode sheets, 16 anode sheets and 18 separators. For both cell formats, a ceramic coated Poly(ethylene terephthalate) fabric with a thickness of 28 µm was used as a separator. Electrodes and separator or, in case of the 3.5 Ah cell, the cell stack was dried at 130°C in a heating vacuum chamber attached to the glovebox equipped with rotary vane pump (specified final pressure: ≤ 10⁻⁴ mbar). The single-layer and multilayer cells were filled with 0.45 mL and 56 mL electrolyte (d = 1.35 g/mL), respectively. After filling, the cells were vacuum sealed and stored for 16 h at 40°C to ensure proper wetting of separator and electrodes prior to formation. The multi-layer cell was evacuated after formation prior to long-term cycling.

Electrochemical Characterisation

In order to obtain potential curves and initial capacities, four formation cycles were applied. In the NVP/C vs. Na half-cells and NVP/C vs. HC full-cells a voltage window of 2.3–3.9 V was used. Charging was performed with constant current (CC) at C/10 until the upper cut-off voltage was reached with subsequent charging at

Table 7. Layout and details on the assembly of the four different research cell formats for the round robin study.

	A 02	B 02	C 02	A 03	B 03	C 03	A 04	B 04	C 04	A 05	B 05	C 05
Cell Type	2E Patt				2E Swagelok				2E Coin			
Configuration	Two-Electrode				Two-Electrode				Two-Electrode			
Setup	half-cell	full-cell	half-cell	half-cell	full-cell	half-cell	full-cell	half-cell	half-cell	half-cell	full-cell	full-cell
Working Electrode	HC	NVP/C	NVP/C	HC	NVP/C	NVP/C	HC	NVP/C	NVP/C	HC	NVP/C	NVP/C
WE Diameter [mm]	14.0		18.0	11.00			15.00		16.00	12.00		
Counter Electrode	Na (d = 0.45 mm)		HC	Na (d = < 1 mm)		HC	Na (d = 0.45 mm)		HC	Na (d = 1 mm)		HC
CE Diameter [mm]	15.60		18.0	11.00			15.60		16.00	12.00		
Reference Electrode	≈ Counter Electrode				≈ Counter Electrode				≈ Counter Electrode			
Separator	QMA		GF/B	GF/B (Whatman)			QMA (Whatman)			2xGF/D (Whatman)		
Sep. Diameter [mm]	22.0		19.0	12.00			16.5			13.0		
Electrolyte	Type A		Type B	Type A	Type B	Type A	Type B	Type B	Type A	Type A	Type B	
Electrolyte Volume [µL]	280		300	100			140		110	500		

constant voltage (CV) until the current dropped below C/20. The discharge was performed using CC of C/10 ending at the lower cut-off voltage. Finally, the cells were charged to 3.0 V using C/10 CC for storage until the next cell test was performed. For the HC vs. Na half-cells, the same protocol was applied, except for the deviating voltage window of 0.005–2 V. CC charging was applied until reaching 0.005 V with CV-phase until $I < C/20$, followed by CC discharging to 2 V. Two different voltage measuring methods were applied for the half-cells: the voltage cut-off was either controlled based on the potential difference of the working electrode against the reference electrode (for 3E Swagelok cells) or working electrode against counter electrode (all other cell types). The C-rate for formation was defined based on the individual active material content of the respective electrode. For HC half-cells a capacity of 335 mAh/g HC was assumed. For the NVP/C half-cells and for full-cells a capacity of 112 mAh/g NVP was assumed. For the subsequent cycling stability tests C-rates were adapted based on the actual cell capacity of its fourth C/10 discharge formation cycle.

In order to obtain data on the full-cell cycling stability for each cell format, 100 cycles applying a current of 0.5 C CC charging with CV until $I < C/10$ and 0.5 C CC discharge were then conducted. In addition, in the multi-layer pouch cell, the internal resistance was measured before and after the cycle stability test. Therefore, a direct current internal resistances (RiDC) test at six different stages of charge (SOCs), namely 10%, 30%, 50%, 70%, 90% and 100%. SOCs were adjusted by Ah-counting based on the determined cell capacity just before the test was used. The RiDCs were measured by use of current pulses of 1 C in discharge direction for 20 s. Using Ohm's law, the DC internal resistances were determined using the potential drop (difference between the potential at the end of the pulse and the potential in rest state before applying the pulse) and the applied current for the respective pulses. After the 100 cycles stability test, a rate capability test was carried out in the discharge direction with the MLP. Charging was always performed using C/2 CC conditions and ended with a CV-phase (until $I < C/20$). In discharge direction, current rates of C/2, 1 C, 2 C, 5 C, 10 C, 15 C and 20 C and back to C/2 were applied. All C-rates were carried out twice. The cell temperature was measured using a thermal sensor that was placed in the centre of the top of the cell.

The multi-layer pouch cell was formatted and cycled using a BaSyTec XCTS 50 A system and the cell was tested in an air-conditioned room at 25 °C ($\pm 2^\circ\text{C}$). All other cells were tested in climate chambers at 25 °C ($\pm 0.1^\circ\text{C}$). During rate capability testing the current at 20 C exceeded 50 A (70.8 A), which is why two BaSyTec XCTS MKII 40 A channels were connected in parallel before testing. For the single-layer pouch cell, a BaSyTec CTS LAB instrument was used. The small-format cells of the round robin study were tested using a Biologic VPM 3 for all half-cells. The round robin full-cells mainly were tested also using the Biologic VPM3, with exception of the 2032 coin cells and 2-electrode Swagelok cells, which were tested on a VPM-300 due to the lack of VPM3 channels for the long-term cycling stability tests.

Author Contributions

Conceptualization, P.St., A.S.; methodology, P.St., A.K., S.K.; investigation, P.St., C.M., N.B., M.M., A.H., T.A., J.K., H.G.; resources, A.H., W.S., P.Sc., A.K., M.S., J.R.B., A.S.; data curation, P.St., M.M., H.G., A.K., D.R., A.S.; writing—original draft preparation, P.St., H.G., A.S.; writing—review and editing, P.St., C.M., A.S. (lead) N.B., M.M., A.H., T.A., J.K., A.K., S.K., D.R., H.G., W.S., P.Sc., M.S., J.R.B. (supporting); visualization, P.St., A.K.; funding acquisi-

tion, A.H., A.K., W.S., P.Sc., J.R.B., A.S. All authors have read and agreed to the published version of the manuscript.

Acknowledgements

We would like to thank Olivia Wiegand for assembly of the multi-layer pouch cell and Steffen Jokisch for support in contacting/electrochemical cycling of the cells. Further, we would like to thank Dr. Thomas Bergfeldt (KIT, IAM-AWP) for the chemical analysis of the NVP/C active material. This work was funded by the Deutsche Forschungsgemeinschaft (DFG, German Research Foundation) under Germany's Excellence Strategy - EXC 2154 - Project number 390874152 (POLIS Cluster of Excellence), and contributes to the research performed at Center for Electrochemical Energy Storage Ulm Karlsruhe (CELEST). Open Access funding enabled and organized by Projekt DEAL.

Conflict of Interests

The authors declare no conflict of interest.

Data Availability Statement

The data that support the findings of this study are openly available in Zenodo at <https://doi.org/10.5281/zenodo.12165686>, reference number 12165686.

Keywords: Sodium-ion battery • NVP • Hard carbon • Round robin • Cell development

- [1] C. Wu, Y. Yang, Y. Zhang, H. Xu, X. He, X. Wu, S. Chou, *Chem. Sci.* **2024**, *15*, 6244.
- [2] P. Gupta, S. Pushpananth, M. A. Haider, S. Basu, *ACS Omega* **2022**, *7*, 5605.
- [3] S. Roberts, E. Kendrick, *Nanotechnol. Sci. Appl.* **2018**, *11*, 23.
- [4] J. Klemens, A.-K. Wurba, D. Burger, M. Müller, W. Bauer, S. Büchele, O. Leonet, J. A. Blázquez, I. Boyano, E. Ayerbe et al., *Batteries Supercaps* **2023**, *6*, e202300291.
- [5] J. Klemens, L. Schneider, D. Burger, N. Zimmerer, M. Müller, W. Bauer, H. Ehrenberg, P. Scharfer, W. Schabel, *Energy Tech.* **2023**, *11*, 2300338.
- [6] a) W. Bauer, M. Müller, L. Schneider, M. Häringer, N. Bohn, J. R. Binder, J. Klemens, P. Scharfer, W. Schabel, H. Ehrenberg, *Nanomaterials (Basel, Switzerland)* **2024**, *14*, 134; b) J. Klemens, L. Schneider, E. C. Herbst, N. Bohn, M. Müller, W. Bauer, P. Scharfer, W. Schabel, *Energy Tech.* **2022**, *10*, 2100985.
- [7] K. M. Abraham, *ACS Energy Lett.* **2020**, *5*, 3544.
- [8] A. Bauer, J. Song, S. Vail, W. Pan, J. Barker, Y. Lu, *Adv. Energy Mater.* **2018**, *8*, 1702869.
- [9] Y. Zhao, Y. Kang, J. Wozny, J. Lu, H. Du, C. Li, T. Li, F. Kang, N. Tavajohi, B. Li, *Nat. Rev. Mater.* **2023**, *8*, 623.
- [10] P. Desai, J. Huang, D. Foix, J.-M. Tarascon, S. Mariyappan, *J. Power Sources* **2022**, *551*, 232177.
- [11] a) N. Tapia-Ruiz, A. R. Armstrong, H. Alptekin, M. A. Amores, H. Au, J. Barker, R. Boston, W. R. Brant, J. M. Brittain, Y. Chen, et al., *J. Phys. Energy* **2021**, *3*, 31503; b) N. Yabuuchi, K. Kubota, M. Dahbi, S. Komaba, *Chem. Rev.* **2014**, *114*, 11636; c) X. Dou, I. Hasa, D. Saurel, C. Vaalma, L. Wu, D. Buchholz, D. Bresser, S. Komaba, S. Passerini, *Mater. Today* **2019**, *23*, 87.
- [12] J. T. Frith, M. J. Lacey, U. Ulissi, *Nat. Commun.* **2023**, *14*, 420.
- [13] Y. Cao, M. Li, J. Lu, J. Liu, K. Amine, *Nat. Nanotechnol.* **2019**, *14*, 200.

- [14] P. Johansson, S. Alvi, P. Ghorbanzade, M. Karlsmo, L. Loaiza, V. Thangavel, K. Westman, F. Årén, *Batteries Supercaps* **2021**, *4*, 1785.
- [15] N. M. Vargas-Barbosa, *Nat. Nanotechnol.* **2024**, *19*, 419.
- [16] P. Stüble, C. Müller, J. Klemens, P. Scharfer, W. Schabel, M. Häringen, J. R. Binder, A. Hofmann, A. Smith, *Batteries Supercaps* **2024**, *7*, e202300375.
- [17] C. Müller, Z. Wang, A. Hofmann, P. Stüble, X. Liu-Théato, J. Klemens, A. Smith, *Batteries Supercaps* **2023**, *6*, e202300322.
- [18] A. Smith, P. Stüble, L. Leuthner, A. Hofmann, F. Jeschull, L. Mereacre, *Batteries Supercaps* **2023**, *6*, e202300080.
- [19] T. Akçay, M. Häringen, K. Pfeifer, J. Anhalt, J. R. Binder, S. Dsoke, D. Kramer, R. Möning, *ACS Appl. Energy Mater.* **2021**, *4*, 12688.
- [20] Q. Zhu, X. Chang, N. Sun, R. Chen, Y. Zhao, B. Xu, F. Wu, *ACS Appl. Mater. Interfaces* **2019**, *11*, 3107.
- [21] D. Balzar, *J. Appl. Crystallogr.* **1992**, *25*, 559.
- [22] M. Häringen, H. Geßwein, N. Bohn, H. Ehrenberg, J. R. Binder, *ChemElectroChem* **2024**, *11*, e202300401.
- [23] Kuranode Co., Ltd., "kuraray KURANODE™ BIOHARDCARBON. Anode Material for Secondary Batteries", can be found under https://cdn.shopify.com/s/files/1/0562/5705/2832/files/KN-brochure-EN-002_1.pdf, **2022**.
- [24] T. Mandai, U. Tanaka, S. Kimura, *Adv. Energy Sustainability Res.* **2024**, 2400059.
- [25] R. Nölle, K. Beltrop, F. Holtstiege, J. Kasnatscheew, T. Placke, M. Winter, *Mater. Today* **2020**, *32*, 131.
- [26] EL-CELL GmbH, "PAT-Cell data sheet. 11-2023", can be found under <https://www.el-cell.com/products/test-cells/standard-test-cells/pat-cell/>, **2023**.
- [27] N. Brandt, L. Griem, C. Herrmann, E. Schoof, G. Tosato, Y. Zhao, P. Zschumme, M. Selzer, *Data Sci. J.* **2021**, *20*, 8.
- [28] D. Grijalva Garces, S. Strauß, S. Gretzinger, B. Schmieg, T. Jüngst, J. Groll, L. Meinel, I. Schmidt, H. Hartmann, K. Schenke-Layland et al., *Biofabrication* **2023**, *16*, 015002.
- [29] a) P. Kraus, E. H. Wolf, C. Prinz, G. Bellini, A. Trunschke, R. Schlögl, *Digital Discovery* **2022**, *1*, 241; b) P. Kraus, N. Vetsch, C. Battaglia, *JOSS* **2022**, *7*, 4166.
- [30] a) P. Sefton, E. Ó Carragáin, S. Soiland-Reyes, O. Corcho, D. Garijo, R. Palma, F. Coppens, C. Goble, J. M. Fernández, K. Chard, et al., *RO-Crate Metadata Specification 1.1.3*, Zenodo **2023**, 10.5281/zenodo.3406497; b) S. Soiland-Reyes, P. Sefton, M. Crosas, L. J. Castro, F. Coppens, J. M. Fernández, D. Garijo, B. Grüning, M. La Rosa, S. Leo, et al., *DS* **2022**, *5*, 97.
- [31] a) S. Clark, F. L. Bleken, S. Stier, E. Flores, C. W. Andersen, M. Marcinek, A. Szczesna-Chrzan, M. Gaberscek, M. R. Palacin, M. Uhrin, et al., *Adv. Energy Mater.* **2022**, *12*, 2102702; b) S. Clark, C. W. Andersen, E. Flores, F. L. Bleken, J. Friis, *Meet. Abstr.* **2022**, MA2022-02, 2582.
- [32] E. Ghedini, G. Goldbeck, J. Friis, A. Hashibon, G. Schmitz, "Elementary Multiperspective Material Ontology (EMMO)", can be found under <https://emmo-repo.github.io/>.
- [33] P. Stüble, M. Müller, T. Bergfeldt, J. R. Binder, A. Hofmann, *Adv. Sci.* **2023**, *10*, 2301874.
- [34] M. Hashimov, A. Hofmann, *Batteries* **2023**, *9*, 530.
- [35] K. Pfeifer, S. Arnold, J. Becherer, C. Das, J. Maibach, H. Ehrenberg, S. Dsoke, *ChemSusChem* **2019**, *12*, 3312.
- [36] L. Gaopan, M. Yanbing, C. Jiawei, P. Yu, Z. Xiao, W. Fei, D. Xiaoli, X. Yongyao, *Sci. China Chem.* **2024**, *67*, 2240–2247.

Manuscript received: June 21, 2024

Revised manuscript received: July 12, 2024

Accepted manuscript online: July 17, 2024

Version of record online: September 6, 2024